Nontrivial temperature behavior of the carrier concentration in graphene on ferroelectric substrate with domain walls

Anatolii I. Kurchak[1], Anna N. Morozovska[2,3], Eugene A. Eliseev[4], Sergei V. Kalinin[5] and Maksym V. Strikha[1,6]

[1] V.Lashkariov Institute of Semiconductor Physics, National Academy of Sciences of Ukraine, pr. Nauky 41, 03028 Kyiv, Ukraine

[2] Institute of Physics of National Academy of Sciences of Ukraine, pr. Nauky 46, 03028 Kyiv, Ukraine

[3]Bogolyubov Institute for Theoretical Physics, National Academy of Sciences of Ukraine, 14-b Metrolohichna str. 03680Kyiv, Ukraine

[4] Institute for Problems of Materials Science, National Academy of Sciences of Ukraine, Krjijanovskogo 3, 03142 Kyiv, Ukraine

[5] The Center for Nanophase Materials Sciences, Oak Ridge National Laboratory, Oak Ridge, TN 37831

[6] Taras Shevchenko Kyiv National University, Radiophysical Faculty pr. Akademika Hlushkova 4g, 03022 Kyiv, Ukraine

Abstract

This work explores a nontrivial temperature behavior of the carriers concentration, which governs the conductance of the graphene channel on ferroelectric substrate with domain walls that is a basic element for field effect transistors of new generation. We revealed the transition from a single to double antiferroelectric-like hysteresis loop of the concentration voltage dependence that happens with the temperature increase and then exist in a wide temperature range (350 – 500) K. We have shown that the double loops of polarization and concentration can have irregular shape that remains irregular as long as the computation takes place, and the voltage position of the different features (jumps, secondary maxima, etc) changes from one period to another, leading to the impression of quasi-chaotic behavior. It appeared that these effects originate from the nonlinear screening of ferroelectric polarization by graphene carriers, as well as it is conditioned by the temperature evolution of the domain structure kinetics in ferroelectric substrate. The nonlinearity rules the voltage behavior of polarization screening by graphene 2D-layer and at the same time induces the motion of separated domain walls accompanied by the motion of p-n junction along the graphene channel. Since the domain walls structure, period and kinetics can be

controlled by changing the temperature, we concluded that the considered nano-structures based on graphene-on-ferroelectric are promising for the fabrication of new generation of modulators based on the graphene p-n junctions.

I. Introduction

The discovery of graphene by Novoselov and Geim [1, 2] had attracted great attention of the scientific community to the study of 2D structures, focused researchers on finding ways to minimize electronic devices and accelerated the transition to nanoelectronics [3, 4]. The unique properties of graphene make it possible to talk about its potential applications in nanoelectronics, optoelectronics, nanoplasmonics, and various sensoric devices, as evidenced by many publications, including the use of graphene for gas sensors [5], transparent electrodes for photovoltaic [6], the production of high-speed nonvolatile memory based on field-effect transistors (FET) with a graphene channel [7, 8, 9], and much more.

It is well known that the suspended graphene sheets, which have intriguing electronic properties [10, 11, 12, 13, 14, 15], cannot remain completely freestanding in space due to the twisting instability. Therefore, all studies associated with this 2D material are necessarily carried out in combination with supporting electrodes, holders or substrates of various kinds. Among the most common substrates are quartz (or mica) and ferroelectric substrates, at that a pronounced free charge accumulation can take place at the graphene - ferroelectric interface [16, 17]. A large number of studies had focused on layered heterostructures using graphene for non-volatile memory elements (see topical review [18] and refs. therein). However, they mainly addressed the macro characteristics (for the instrument as a whole) inherent in such systems, namely, the appearance of a hysteresis loop of the average concentration of carriers, the width of the memory window, the dependence of the memory window on the switching speed of the gate voltage. However, if we go down one level below and consider the behavior of the carriers when applying an external electric field, their distribution in graphene, the effect of the substrate on the distribution of carriers, then one can obtain more profound knowledge of the processes occurring in the system under applied external electric field. These studies are needed to understand and explain the macro-characteristics for such heterostructures.

One of these examples is the existence of a **p-n-junction** in a graphene channel, which was experimentally implemented on a dielectric SiO_2 substrate [19, 20], at first with the help of a multi-gate system [21]. P-N-junctions in graphene explore the opportunities to observe the physical manifestations of Andreev reflection, Klein tunneling, quantum Hall effect and Veselago lensing [22, 23, 24].

Later on then Hinnefeld et al [25] and Baeumer et al [26] created a p-n-junction in graphene using the ferroelectric substrates Pb(Zr, Ti)O_3 and $LiNiO_3$, respectively. In the case of a ferroelectric substrate, the formation of regions with electron and hole concentration of carriers in the channel arises due to the existence of domains with different directions of polarization [27, 28]. Kurchak et al [29, 30] revealed that adsorbed charges dynamics leads to the hysteresis effect on conductivity in the graphene channel on an organic ferroelectric substrate. Kim et al. [31] propose graphene on ferroelectric for nonvolatile memory and reconfigurable logic-gate operations.

Morozovska et al [32, 33, 34] have shown that the finite-size effects can strongly influence the nonlinear hysteretic dynamics of the stored charge and electro-resistance in the multilayer graphene on ferroelectric with domain stripes of different polarities, which can induce domains with *p*- and *n*-type conductivity, and with p-n-junction potentials at domain walls. Theoretical models for the different types of current regimes (from ballistic to diffusive one) in a single-layer graphene channel at 180^o- ferroelectric domain walls have been developed [35, 36] and it was shown that the domain wall contact with the surface creates p-n junction in graphene channel. Recently thermodynamics and kinetics of the conductance of p-n-junctions induced in graphene channel by stripe domains nucleation, motion and reversal in a ferroelectric substrate has been explored using self-consistent approach based on Landau-Ginzburg-Devonshire (**LGD**) theory combined with classical electrostatics, semiconductor theory and quantum statistics for electrotransport calculations [37] at room temperatures.

Taking into account the above-mentioned theoretical results, it should be emphasized the importance and necessity of considering the dynamics of p-n junctions and the distribution of carrier concentrations along the graphene channel for various types of ferroelectrics in a wide temperature range. Such studies can answer the question about the possibility to create the devices based on graphene on ferroelectric heterostructures operating at different temperatures. To the best of our knowledge the dependence of graphene channel electro-conductance and resistance on ferroelectric substrate properties and domain structure evolution has been studied at room temperature only (see e.g. Refs.[16, 17, 25, 26, 31, 38, 39]). Specifically, hysteresis loops of graphene resistance, which have either ferroelectric-like or antiferroelectric-like shape depending on the top and bottom gate voltages, have been observed in the system graphene-on-ferroelectric substrate [16]. A qualitative and even semi-quantitative agreement of the loops calculated within self-consistent LGD approach with experiments [16, 38] was reached [33, 34]. However the temperature evolution of the carrier concentration have not been studied experimentally or calculated theoretically.

Motivated by above problem, this work explores peculiarities of the carriers concentration temperature behavior, which governs the graphene channel conductance in the nano-structure graphene channel-ferroelectric substrate with domain structure that can be used as a basic element for FETs in advanced non-volatile memory units. We revealed the nontrivial dependences of the concentration hysteresis on temperature and gate voltage amplitude, which exist in the vicinity of ferroelectric transition temperature and far from it. It appeared that the nontrivial peculiarities originate from the temperature evolution of the domain structure kinetics in ferroelectric substrate.

II. Problem geometry and basic equations

System under consideration is similar to one examined in Ref.[37] and its geometry is shown in **Fig.1(a)**. The geometry corresponds to the experiments [16, 17, 25, 26, 31, 38, 39] and includes top gate electrode, top oxide dielectric layer, conducting graphene channel with source and drain electrodes, ferroelectric substrate with top dead layer and bottom electrode.

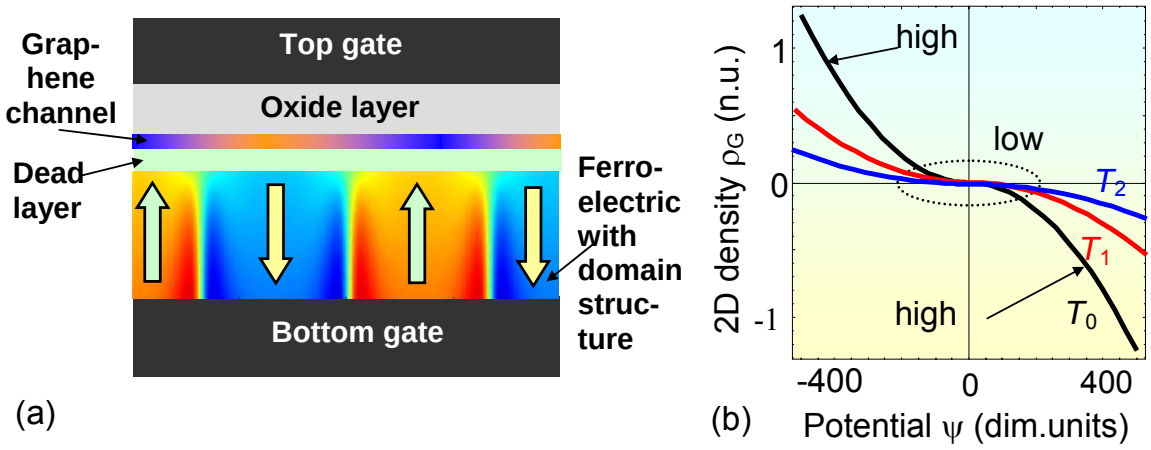

Figure 1. (a) Schematics of the considered nano-hetero-structure consisting of top gate, dielectric oxide layer, graphene channel, ultra-thin paraelectric dead layer, ferroelectric substrate with domain walls and bottom gate electrode. (adapted from [37]) **(b)** Dependence of the 2D charge density of graphene on the dimensionless potential ψ calculated at different temperatures T_0 (black curve), $T_1 = 1.5T_0$ (red curve) and $T_2 = 2T_0$ (blue curve).

The technological requirements and realities of GFETs design are so that the existence of the top oxide and dead layers are unavoidable for most above mentioned experiments [16, 17, 25, 26, 31, 38, 39]. In particular the top oxide layer prevents graphene damage and contamination by the top gate electrode, as well as its thickness should be enough small and dielectric permittivity value should be enough high to prevent the dielectric breakdown [40, 41, 42]. The top oxide layer thickness vary in the range (5 – 50) nm, at that thinner layers should

have higher dielectric permittivity to minimize the probability of the breakdown. The relative dielectric permittivity of top oxide layer can vary in a wide range 4-100 depending on the oxide material [40-42], e.g. it is equal to 4 for SiO_2, 9 - 10 for Al_2O_3, 25-30 for HfO_2 and 80 for TiO_2.

The physical origin of natural dead layer is the unavoidable contamination of electrically-open (i.e. non-electroded) ferroelectric surface that becomes paraelectric aiming to provide maximally efficient electric screening of the polarization bound charge [43, 44]. There are different types of "dead" (or "passive") layers [43, 44], most of them are ultrathin sub-surface layers of thickness less than several nm located under the surface, where the spontaneous polarization is absent (or negligibly small) due to the surface reconstruction, contamination, zero extrapolation length and/or strong depolarization field [43, 44]. Artificial dead layers can be much thicker. The matter in the natural dead layer is of almost the same chemical composition than in the bulk of ferroelectric substrate, but it is in the paraelectric phase induced by the surface confinement effect, and so the relative dielectric permittivity of the dead layer ε_{DL} is usually rather high ~(50 – 500) (as it should be for paraelectrics at room temperature [45]), in comparison with unity for a physical gap. Below the dead layer is treated as a top sub-surface layer of a ferroelectric film being in the paraelectric phase.

Above discussion means that the special attention should be paid to the choice of the dielectric properties and thicknesses of the top oxide and dead layers, because both of them strongly affect on electric potential and field distributions in graphene sheet and ferroelectric substrate. Additionally the dead layer controls the ferroelectric polarization screening and domain structure features [43, 44, 46, 47]. Anyway the electric potential drops in both these layers, and the drop depends on the layers relative dielectric permittivity ε_O and ε_{DL}, and thicknesses h_O and h_{DL}, respectively. In the oxide dielectric and ultrathin dead layers equations of state relating displacement **D** and electric field **E,** are $\mathbf{D} = \varepsilon_0 \varepsilon_O \mathbf{E}$ and $\mathbf{D} = \varepsilon_0 \varepsilon_{DL} \mathbf{E}$, ε_0 is a universal dielectric constant. Electric potentials φ_O and φ_{DL} satisfies Laplace's equation inside the layers. The dielectric permittivity of oxide layer ε_O can vary in a wide range (4-100) depending on the oxide material. The relative dielectric permittivity ε_{DL} of the paraelectric dead layer is regarded rather high ~100. **Appendix A** presents the analytical (**Eqs.(S.7)**) and graphical (**Figs.S1-S3**) results of analytical study of the influence of the parameters h_O, h_{DL}, ε_O and ε_{DL} on the maximal spontaneous polarization value and graphene charge. To study the parameters h_O and h_{DL} effect on the hysteresis loops we performed numerical calculations, which results are shown in **Figs.S4.** The parametric study allows us to select the values of parameters from their physical ranges listed in **Table S1** for further numerical studies of the most interesting

temperature dependences of the carrier concentration and ferroelectric polarization in the considered nanostructure.

A planar single-layer graphene channel is characterized by the two-dimensional (2D) electron density of states, $g_n(\varepsilon)=g_p(\varepsilon)=2\varepsilon/\left(\pi\hbar^2 v_F^2\right)$ (see e.g. [48, 49]). Corresponding graphene charge density $\sigma_G(\psi)=e\left(p_{2D}(\psi)-n_{2D}(\psi)\right)$ is the difference of 2D concentrations of electrons in the conduction band [$n_{2D}(\varphi)=\int_0^\infty d\varepsilon g_n(\varepsilon)f\left(\varepsilon-E_F-e\varphi\right)$] and holes in the valence band [$p_{2D}(\varphi)=\int_0^\infty d\varepsilon g_p(\varepsilon)f\left(\varepsilon+E_F+e\varphi\right)$], respectively (E_F is a Fermi energy level, these expressions correspond the gapless graphene spectrum). Corresponding expression for $\sigma_G(\psi)$ and its Pade-exponential approximation derived in Ref.[37] is

$$\sigma_G(\psi)=\frac{4(k_BT)^2 e}{\pi\hbar^2 v_F^2}\sum_{m=1}^{\infty}\frac{(-1)^m}{m^2}\sinh(m\psi)\approx\frac{2(k_BT)^2 e}{\pi\hbar^2 v_F^2}\left(\frac{1}{\eta(\psi)}-\frac{1}{\eta(-\psi)}\right), \qquad (1)$$

where the functions are $\psi=\frac{e\varphi+E_F}{k_BT}$ and $\eta(\psi)=\exp(\psi)+2\left(\psi^2+\frac{\psi}{2}+\frac{2\pi^2}{12-\pi^2}\right)^{-1}$. The dependence of $\sigma_G(\psi)$ on the dimensionless voltage ψ is shown in **Fig.1(b).**

As a substrate for graphene channel we consider a ferroelectric film of thickness *l* with the spontaneous polarization component P_3^f directed along its polar axis z. The film contains 180-degree domain wall – surface junctions [see **Fig. 1(a)**]. The dependence of the transverse polarization components P_1 and P_2 on the field **E** are linear and corresponding relative dielectric permittivities are equal, $\varepsilon_{11}^f=\varepsilon_{22}^f$. Polarization z-component is $P_3\left(\mathbf{r},E_3\right)=P_3^f\left(\mathbf{r},E_3\right)+\varepsilon_0\left(\varepsilon_{33}^b-1\right)E_3$, where a so-called relative "background" permittivity ε_{ij}^b~(4 – 7) is introduced [43, 50]. The distribution of $P_3^f(x,y,z)$ is determined from the time-dependent LGD type Euler-Lagrange equation,

$$\Gamma\frac{\partial P_3^f}{\partial t}+a(T)P_3^f+b\left(P_3^f\right)^3+c\left(P_3^f\right)^5-g\Delta P_3^f=E_3. \qquad (2)$$

Γ is a Landau-Khalatnikov relaxation coefficient [51], $a(T)=\alpha_T\left(T-T_C\right)$, T is the absolute temperature, T_C is a Curie temperature of a bulk ferroelectric, *b* and *c* are the coefficients of LGD potential expansion on the polarization powers (also called as linear and nonlinear dielectric stiffness coefficients), *g* is a gradient coefficient and Δ stands for a 3D-Laplace operator. The boundary conditions are of the third kind [52],

$$\left(P_3^f - \Lambda_+ \frac{\partial P_3^f}{\partial z} \right)\Bigg|_{z=h_D} = 0, \qquad \left(P_3^f + \Lambda_- \frac{\partial P_3^f}{\partial z} \right)\Bigg|_{z=h_{DL}+h_F} = 0 \tag{3}$$

The physical range of extrapolation lengths $\Lambda_\pm$ is (0.5 – 2) nm [53]. Quasi-static electric field is defined via electric potential as $E_3 = -\partial\varphi/\partial z$. The potential φ_f satisfies Poisson equation inside a ferroelectric film.

For the problem geometry shown in the **Fig. 1(a)** the system of electrostatic equations acquires the form:

$$\Delta\varphi_O = 0, \quad \text{for} \quad -h_O < z < 0, \quad \text{(oxide dielectric layer "}O\text{")} \tag{4a}$$

$$\Delta\varphi_{DL} = 0, \quad \text{for} \quad 0 < z < h_{DL}, \quad \text{(dead layer "}DL\text{")} \tag{4b}$$

$$\left(\varepsilon_{33}^b \frac{\partial^2}{\partial z^2} + \varepsilon_{11}^f \Delta_\perp \right)\varphi_f = \frac{1}{\varepsilon_0}\frac{\partial P_3^f}{\partial z}, \quad \text{for} \quad h_{DL} < z < h_{DL} + h_F. \quad \text{(ferroelectric "}f\text{")} \tag{4c}$$

3D-Laplace operator is Δ, 2D-Laplace operator on transverse coordinates {x,y} is $\Delta_\perp$. Boundary conditions to Eqs.(4) are as follows: the fixed potential at the top gate, $\varphi_O(x, y, z = -h_O) = U(t)$ and zero potential at the bottom gate $\varphi_f(x, y, z = h_{DL} + h_F) = 0$; the continuity of the electric potential at the graphene layer, $\varphi_O(x, y, 0) = \varphi_{DL}(x, y, 0)$; the equivalence of difference of the electric displacement normal components, and $D_3^{DL} = \varepsilon_0\varepsilon_{DL}E_3$, to the surface charges in graphene $\sigma_G(x, y)$, $D_3^O(x, y, 0) - D_3^{DL}(x, y, 0) = \sigma_G(x, y, \varphi)$; and the continuity of the potential and displacement normal components, $D_3^f = \varepsilon_0\varepsilon_{33}^b E_3 + P_3^f$ and, at dead layer/ferroelectric interface, $\varphi_{DL}(x, y, h_{DL}) = \varphi_f(x, y, h_{DL})$ and $D_3^{DL}(x, y, h_{DL}) - D_3^f(x, y, h_{DL}) = 0$. Electric displacements are $D_3^O = \varepsilon_0\varepsilon_O E_3$, $D_3^{DL} = \varepsilon_0\varepsilon_{DL}E_3$ and $D_3^f = \varepsilon_0\varepsilon_{33}^b E_3 + P_3^f$. The gate voltage is periodic with a period T_g, $U(t) = U_{\max}\sin(2\pi t/T_g)$. Periodic boundary conditions were applied in x-direction.

To resume this section we would like to underline that the problem (1)-(4) is coupled, because the LGD (2) and electrostatic equations (4) couple electric field and polarization. Actually the polarization P_3 in a ferroelectric depends on the electric field E_3 [see Eq.(2)]. In turn the field E_3 strongly depends on the carrier concentration (1) in graphene $\sigma_G(x, y, \varphi)$ and dielectric layer properties via the boundary condition $D_3^O(x, y, 0) - D_3^{DL}(x, y, 0) = \sigma_G(x, y, \varphi)$. In accordance with Eq.(1) the concentration $\sigma_G(x, y, \varphi)$ in ruled by the electric potential φ, which in turn depends on the polarization value and its gradient according to Eqs.(4) with above-listed electric boundary conditions. Hence the coupled equations (1)-(4) self-consistently describe the influence of electric field induced by the ferroelectric domain structure on the graphene

conductivity, as well as the influence of graphene top electrode on the domain structure in a ferroelectric. The direct sequences of the mutual graphene-ferroelectric influence are (i) the appearance of p-n junctions in graphene at FDW [30, 35, 36, 37], (ii) the broadening of the domain walls near the ferroelectric surfaces [54] appearing to minimize the depolarization electric field energy [as shown in Fig.1(a)] and unusual temperature evolution of the ferroelectric polarization switching and hysteresis loops of charge density in graphene, which will be presented and analyzed in next sections.

Notably the used self-consistent approach "LGD + electrostatics" is well-recognized for calculations of local polarization dynamics at ferroelectric interfaces [55]. The approach coupling ferroelectric polarization, electric field and surface and/or space charge are the basis for phase-field simulations and finite element modelling of the polarization reversal and domain structure evolution in ferroelectric nano-grained ceramics, thin films and their graded structures (see e.g. seminal papers of L.Q. Chen group [56, 57], P. Alpay group [58, 59, 60] and J. F. Scott group [61, 62]).

III. Influence of ferroelectric domain structure on the carrier concentration in graphene channel at different temperatures

Below we present results of numerical modeling of the problem (1)-(4). We study numerically the modulation of the carrier concentration, which governs the graphene channel conductance caused by a domain structure moving in a ferroelectric substrate. Parameters used in the calculations are listed in **Table SI.**

Plots in **Fig. 2** show the spatial distribution of polarization in a 75-nm thick ferroelectric substrate calculated at several temperatures within the range (300 – 500)K and gate voltages U_{max} = 2V **(a)** and 10 V **(b)**. From **Figs.2** the maximal polarization and domain structure contrast decreases with temperature increase, and the broadening of the domain walls increases near the substrate-gap interface. From **Fig.2(a)** the domain period decreases with temperature increase. At 300 K the domain structure is relatively contrast in comparison with the faint image at 500 K for U_{max} = 2 V. The domain period is almost temperature-independent in **Fig.2(b)**, but ferroelectric domain structure disappears at 500 K for U_{max} = 10 V.

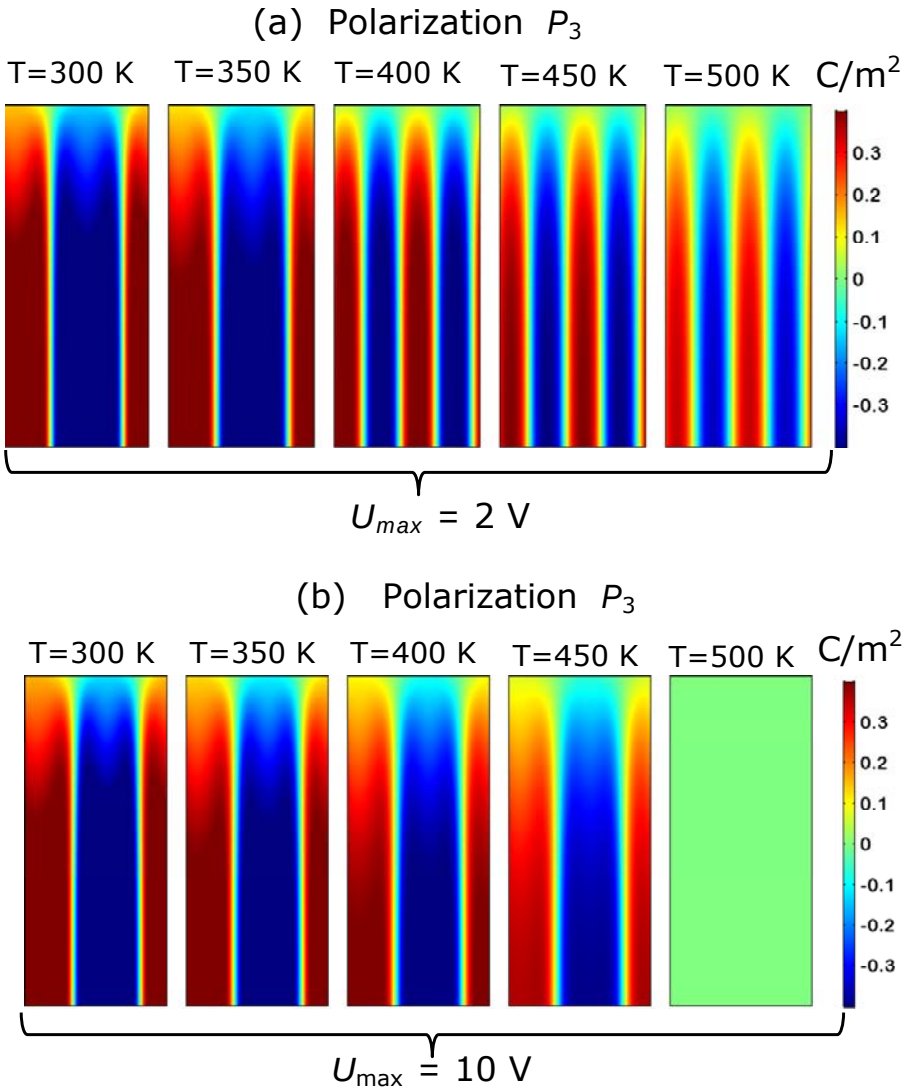

Figure 2. Spatial distribution of a ferroelectric polarization component P_3 calculated for different temperatures 300, 350, 400, 450 and 500 K (legends at the plots); Snapshot of domain structure was done at moment of time t=T_g=1000 s. The gate voltage amplitude U_{max} = 2 V **(a)** and U_{max} = 10 V **(b)**. Parameters are listed in **Table SI.**

The nontrivial question to **Fig.2** is why ferroelectric domain structure disappears at 500 K for U_{max} = 10 V, but still exists at U_{max} = 2 V? A possible answer is that applied voltage increases the degree of the substrate unipolarity and supports the ferroelectric single-domain state [37]. Note that the transition temperature of the single-domain ferroelectric substrate into a non-polar paraelectric phase decreases under the thickness decrease; it is about 500 K for a 70 nm film at U_{max} = 0 and chosen material parameters. The critical thickness is much smaller for the poly-domain films [63]. So that increasing U_{max} leads to the film unipolarity and increases its critical thickness at the same time.

The spatial-temporal evolution of the domain structure defines the evolution of the carrier concentration $\Delta n_G(x,t)$ in the graphene channel; at that a separate p-n junction is located above

each domain wall [35-37]. To illustrate this, **Figs 3** show x-profiles of the $\Delta n_G(x,t)$ calculated along the graphene channel at several temperatures within the range (300 – 500)K and gate voltages $U_{max} = 2$V **(a)** and 10 V **(b)**. Positive $\Delta n_G(x,t)$ correspond to holes, and negative to electrons. The amplitude of $\Delta n_G(x,t)$ is maximal for room temperature 300 K, monotonically and strongly decreases with temperature increasing; then it almost [**Fig.3(a)**] or completely [**Fig.3(b)**] vanishes at 500 K. The amplitude decrease is in agreement with the temperature decrease of maximal polarization in the central regions of domains, $P_S \sim \sqrt{T_C - T}$. The modulation amplitude is almost the same at $U_{max} = 2$V and 10 V.

There are two p-n junctions at (300-350) K located at distance 15 nm; and four p-n junctions at (400-450) K at $U_{max} = 2$V [**Fig.3(a)**]. The temperature-dependent number of p-n junctions is determined by the corresponding number of domain walls, which doubles with the temperature increase from 300 K to 400 K [**see Fig.3(a)**]. For the reasons described above [see **Fig.2(b)** and comments] the amount of p-n junctions does not change with temperature increase from 300 to 450 K at $U_{max} = 10$V [see black, red, magenta and blue curves in **Fig.3(b)**]. The charge modulation disappears at 500 K, since the domain structure disappears [see the green line in **Fig.3(b)** and plot for 500 K in **Fig.2(b)**].

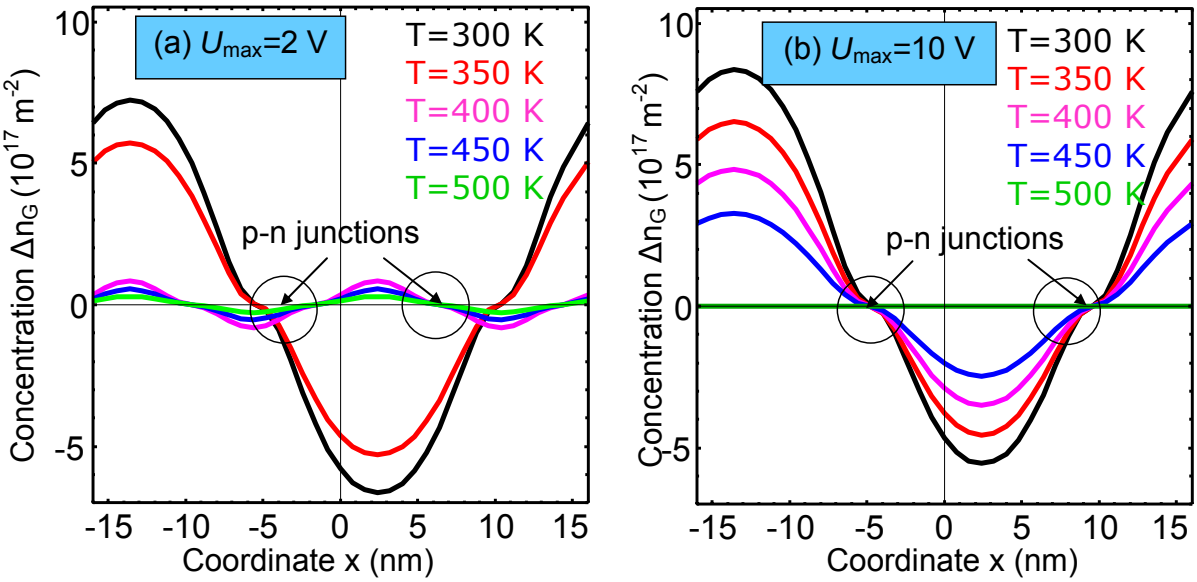

Figure 3. 2D-concentration of the carriers $\Delta n_G(x,t)$ in the graphene channel calculated for different temperatures 300, 350, 400, 450 and 500 K (different curves) at time moment t=T_g=1000 s. The gate voltage amplitude $U_{max} = 2$ V **(a)**and $U_{max} = 10$ V **(b)**. P-N junctions are marked by circles. Parameters are listed in **Table SI.**

Color maps in **Figs 4(a)** and **4(b)** illustrate the temporal evolution of the 2D-concentration of carriers x-profile in graphene channel ($\Delta n_G(x,t)$) for the temperatures 300 K and 400 K, respectively. It is seen that the periodic changes of $\Delta n_G(x,t)$ correlate with the number of domain walls in a ferroelectric substrate that doubles with temperature increasing from 300 K to 400 K. At that the amplitude of $\Delta n_G(x,t)$ decreases in an order of magnitude (from 10^{18}m^{-2} to 10^{17}m^{-2}) with the temperature increasing from 300 K to 400 K.

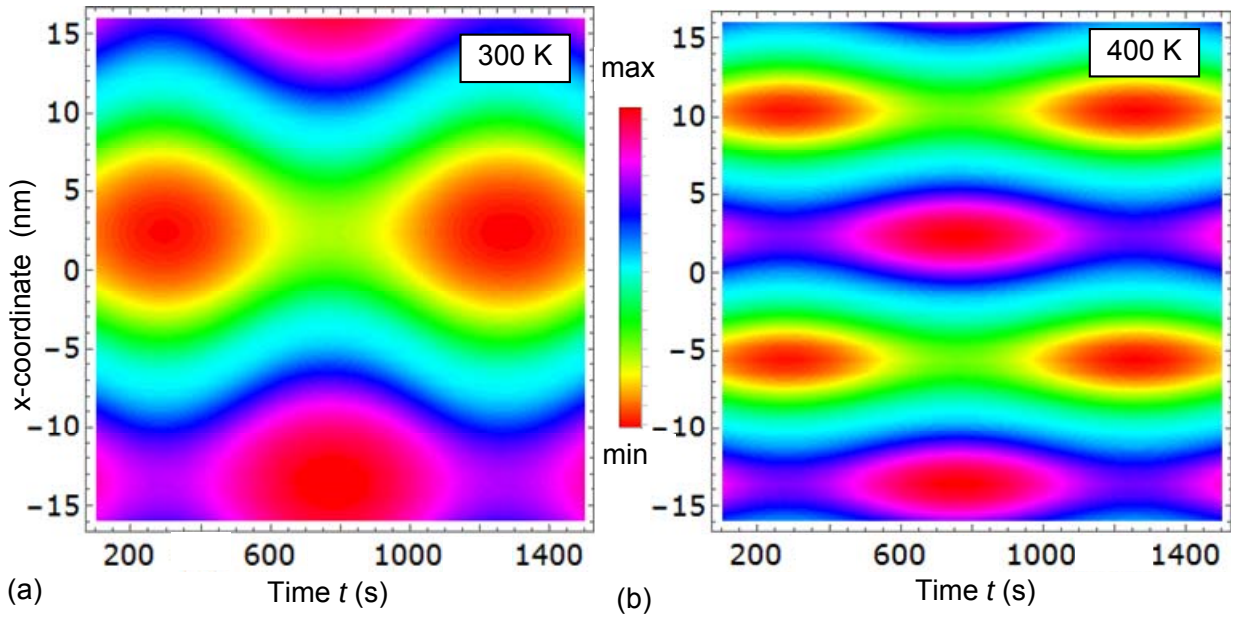

Figure 4. Spatial-temporal evolution of the 2D-concentration of carriers in graphene channel calculated for different temperatures 300 K **(a)** and 400 K **(b)**. The gate voltage amplitude U_{max} = 2 V. Color scale changes from ±10^{18}m^{-2} for 300 K to ±10^{17} m^{-2} for 400 K. Parameters are listed in **Table SI.**

Color maps in **Figs 5(a)** and **5(b)** show the temperature changes of the 2D-carriers x-profile calculated for two temperature ranges, (300 – 400) K and (300 – 560) K, respectively. It is seen that the contrast of $\Delta n_G(x,t)$ monotonically decreases in an order of magnitude (from 10^{18}m^{-2} to 10^{17}m^{-2}) with the temperature increasing from 300 K to 560 K. The number of minima and maxima correlates with the number of domain walls in a ferroelectric substrate that doubles with temperature increasing from 300 K to 400 K [see **Fig. 3(a)** and **3(b)**].

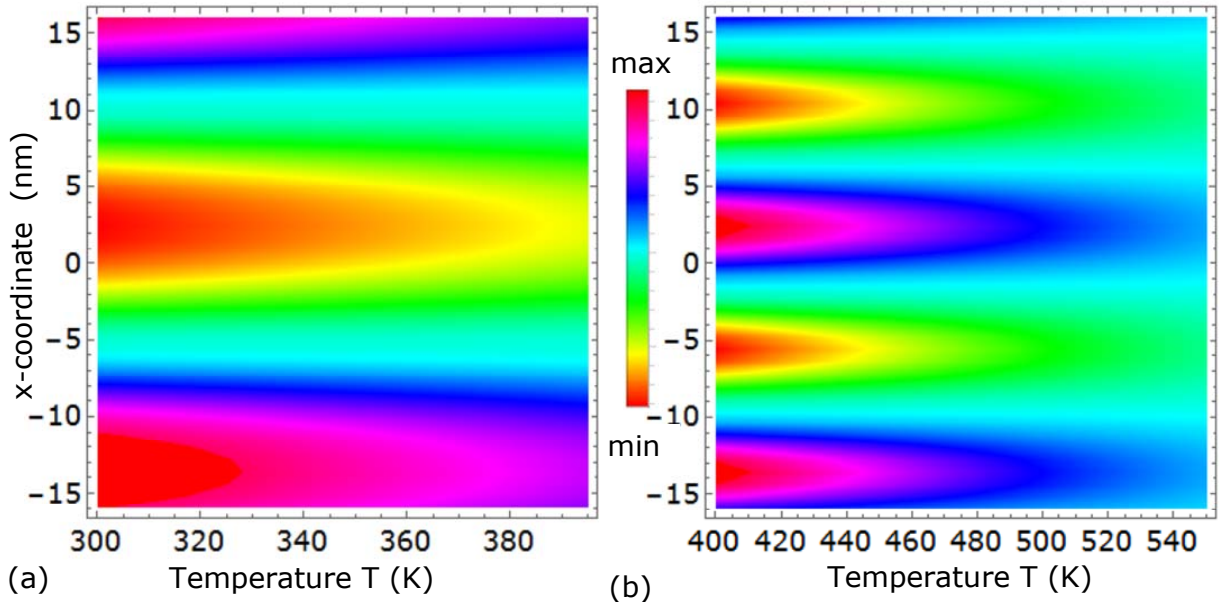

Figure 5. Spatial-temperature distribution of the 2D-concentration of carriers in graphene channel calculated for the temperature ranges (300 – 400) K **(a)** and (400 – 560) K **(b)**. The gate voltage amplitude $U_{max} = 2$ V. Color scale changes from $\pm 10^{18} m^{-2}$ for 300 K to $\pm 10^{17}$ m^{-2} for 400 K. Parameters are listed in **Table SI.**

IV. Hysteretic response of average carrier concentration in graphene channel

The dependence of the average concentration of carriers in graphene channel on the voltage applied to the gate is hysteretic and temperature-dependent [see the right column in **Fig.6**]. At that the concentration loops are very different from the average polarization loops at small amplitudes of the gate voltage $U_{max} \le 10$ V [compare **Fig.6(a)** with **6(b)**]**.** In particular the concentration loop has a pronounced single hysteresis shape with ending characteristic for the conductivity contribution at room temperature and $U_{max} = 10$ V. The loop becomes lower and slightly thinner at 450 K, then it transforms into a very slim double-shape loop at 500 K (see different loops in **Fig.6(b)** and Ref.[37]). Corresponding polarization loops are very slim in the actual temperature and gate voltage range $U_{max} \le 10$ V as anticipated for a multi-domain scenario of polarization reversal (see different loops in **Fig.6(a)** and Ref.[37]). Hence the transformation of the concentration loop with the temperature increase is dictated by the domain structure dynamics at $U_{max} \le 10$ V, rather then by the ferroelectric polarization loop changes, and the relation occurs in a non-proportional way.

Notably the polarization loop shape changes from the slim one and to a pronounced square-like hysteresis with the gate voltage amplitude increase to 15V and temperatures $T \le 320$ K [see orange and red loops in **Figs. 6(c)**]**.** At $T \le 320$ K the temperature behavior of

square-like concentration loops is dictated by the almost single-domain polarization reversal at $U_{\max} \geq 10$ V, but the relation occurs in a non-proportional way [see orange and red loops in Figs. **6(d)**].

With the temperature increase above 320 K the double antiferroelectric-like hysteresis loops of polarization and concentration appear, undergoing unusual shape changes (additional flexures and maxima) and exist in a wide temperature range $320 \leq T \leq 500$ K [compare magenta, blue, dark green and light green loops in **Figs. 6(c)** and **6(d)**]. The height and width of the double loops decreases with the temperature increase, and minor loops by-pass is counterclockwise [see magenta, blue, dark green and light green loops in **Figs. 6(e)** and **6(f)**]. These double antiferroelectric-like loops of polarization and concentration disappear at approximately (500 - 550) K indicating the transition of the ferroelectric substrate to a paraelectric phase [see green and black linear curves in **Figs. 6(c)-(f)**].

Note that the wide temperature range of the double loop existence (about 180 K) is at least 10 times more that the range of double hysteresis loops existence in the ferroelectric with the first order phase transition to a paraelectric phase. The physical origin of the double antiferroelectric-like loops can be explained by the voltage behavior of the graphene charge density shown in **Fig.1(b)** for different temperatures. The dependence becomes significantly steeper with the temperature decrease**.** Since the graphene charge is responsible for the polarization screening in a ferroelectric substrate, high charge densities (corresponding to high acting electric potential $|e\varphi| >> k_B T$ and lower temperatures) can provide an effective screening, and the low ones (corresponding to small potentials $|e\varphi| \leq k_B T$ and higher temperatures) can provide a weak incomplete screening only. At low enough temperatures ($T \leq 320$ K) the substrate (PZT film of thickness 75 nm) is in a deep ferroelectric phase, and relatively weak screening of its depolarization field by graphene sheet is enough to support the ferroelectricity in it. Corresponding hysteresis loop is a single one, has a square-like shape with relatively high remanent polarization and coercive voltage. The situation principally changes with the temperature increase, since the film approaches the paraelectric transition. The transition happens at 666 K for a bulk sample, for thin films it happens at much lower temperatures and strongly depends on the film thickness and screening conditions in a self-consistent way [63, 64, 65, 66]. At that the better the screening the higher is the critical thickness of the transition [63, 65, 66]. Thus additional screening by graphene carriers is urgently required to maintain the thin film in a ferroelectric state. As one can see from **Fig.1(b)** the screening increase appears at nonzero potential φ that is in turn proportional to the gate voltage U. The critical voltage corresponding to the screening degree enough to suppress the thickness-induced paraelectric

transition opens the minor loops of polarization, which in turn induce the concentration loops of anti-hysteretic type.

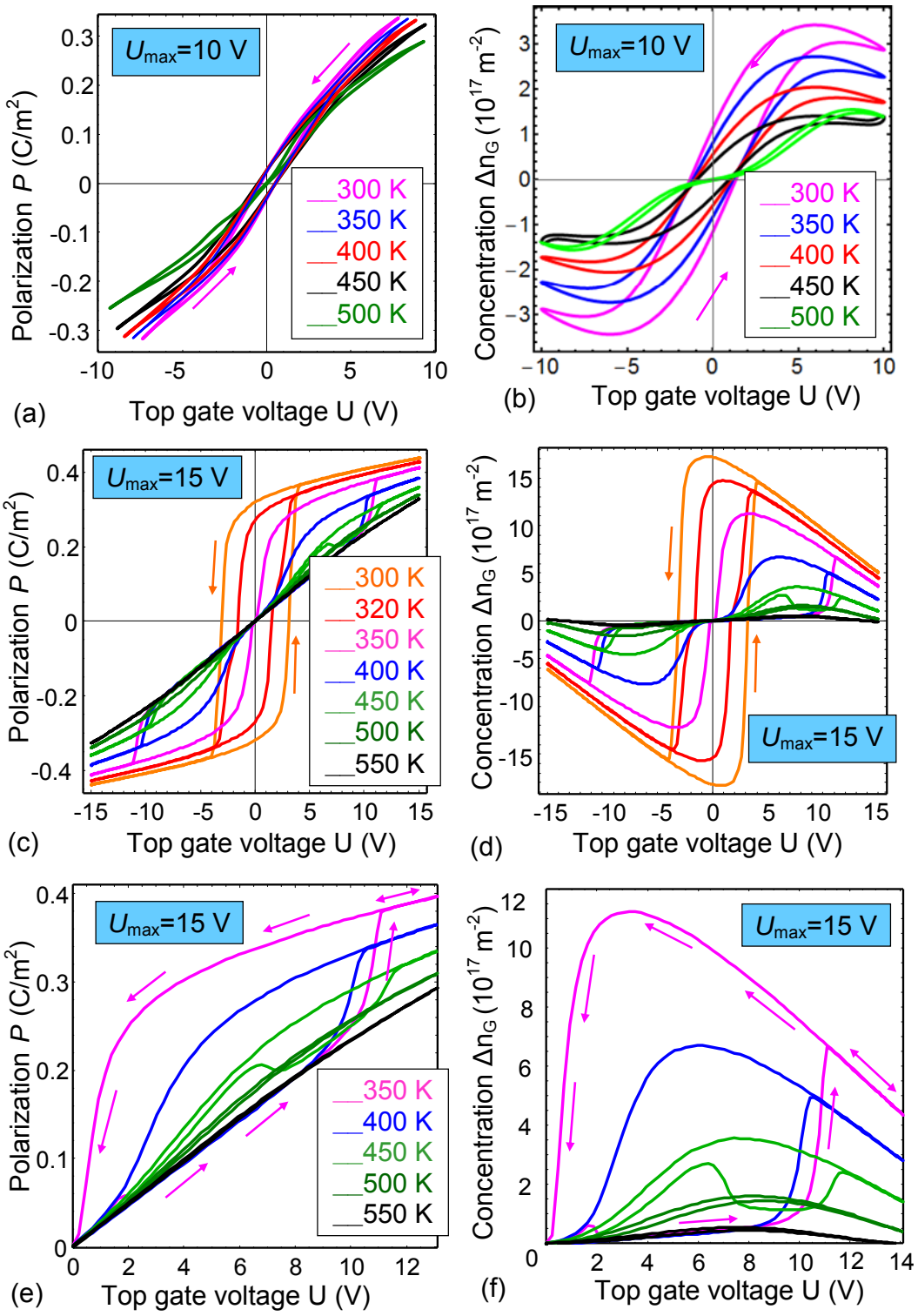

Figure 6. Hysteresis loops of the average polarization $P(U)$ of ferroelectric substrate **(a, c, e)** and carriers concentration variation in graphene channel $\Delta n_G(U)$ **(b, d, f)** calculated for different temperatures (different curves), U_{max} = 10 V **(a, b)** and U_{max} = 15 V **(c, d, e, f);** T_g=1000 s. Other parameters are listed in **Table SI.** Arrows indicate the counterclockwise direction of the loops by-pass.

Plots **(e)** and **(f)** show positive one-half of the double hysteresis loops calculated at 350, 400, 450, 500 and 550 K(different curves), U_{max} = 15 V.

Single loops of polarization and conductivity (such as shown in **Figs.6**), which correspond either to poly-domain [**Fig.6(a,b)**] or to the monodomain [**Fig.6(c,d)**] scenario of polarization reversal, always have regular shape [see **Figs.7(a)**]. However the double loops, which have regions with poly-domain states at definite temperatures, can be or regular or irregular shape [compare **Figs.7(b)** and **7(c)**].

Single and double hysteresis loops, which have a regular shape (symmetric or anti-symmetric), are reproducible at every period of applied voltage, as anticipated. Quite unexpectedly we revealed the double hysteresis loops of polarization and concentration, which have irregular shape, are "superperiodic" in the sense that they are reproduced only after a great amount of the voltage periods [**Figs.7(c)**]. An example of ten period "superperiodic" polarization and concentration double loops of irregular shape are shown in **Figs.7(d)** and **Figs.7(e)**, respectively. The wording "superperiodicity" in the considered case means that the double loop shape remains irregular as long as the computation takes place, and the voltage position of the different features (jumps, secondary maxima, etc.) changes from one period to another, leading to the impression of quasi-chaotic behavior. We established that the physical origin of the "quasi-chaotic" behavior of the polarization and concentration double loops is the strongly nonlinear voltage behavior of the graphene screening charge [see Eq.(1) and **Fig.1(b)**]. The nonlinearity rules the voltage behavior of polarization screening by graphene 2D-layer and at the same time induces the motion of separated domain walls accompanied by the motion of p-n junction along the channel. However these speculations do not account for the lattice pinning effect on the domain wall motion, that can decrease the velocity of domain walls on several orders of magnitude [67]. On the other hand the local excitation by the probe electric field opens the possibilities for intrinsic switching of polarization [68, 69] and correlated nucleation of domains [70] and so the quasi-free motion of domain walls are far not excluded in thin films.

To quantify the anomalous temperature behavior of the polarization and graphene carriers concentration loops we calculated the temperature dependences of the switchable remanent polarization $2P_R$ (polarization loop height at moments of time which correspond to zero gate voltage value) and concentration $2\Delta n_R$ (concentration loop height at moments of time which correspond to zero gate voltage value) and coercive voltage windows, $2U_{CP}$ and $2U_{CN}$, respectively corresponding to the width of the loops [see designations in **Figs.7(a)**]. For double loops we calculated the temperature dependence of the critical voltage of the minor loops opening, U_{cr} [see designations in **Figs.7(b)**].

Calculation results for polarization and concentration loops parameters are shown in **Figs.8** and **9**, respectively**.** As one can see from the figures, there are functional proportionally between the parameters temperature behavior, namely $P_R(T) \sim \Delta n_R(T)$ and $U_{CP}(T) \sim U_{CN}(T)$, moreover $U_{CP}(T) = U_{CN}(T)$ for a single loops. However for double loops $U_{CP}(T) < U_{CN}(T)$ on a value about 5-2 V, and the difference is temperature dependent [see **Fig.10**].

Different curves in **Figs. 8-9** correspond to different amplitudes of the gate voltage U_{max} = (2, 5, 8, 10, 15) V. Also one can see the pronounced peculiarity related with the transition from the single-domain polarization reversal to a poly-domain one which occurs at U_{max} = 15 V and $T \approx 330$ K (see green curves in **Figs.8-9**). The abrupt at black, red, blue and magenta curves corresponds to the transition from the single loop to the double one. The steps at coercive voltages correspond to the domain structure re-building (such as e.g. abrupt changes of its period) taking place due to the spatial confinement of the film in transverse direction. The zigzag-like oscillations of on the polarization, concentration and their coercive fields temperature dependences originated from the quasi-chaotic behavior of the double loops with irregular shape [such as shown in **Figs.7(d)-(e)**]. Namely, the oscillations correspond to the left- and right-voltage asymmetry of the double loops shape.

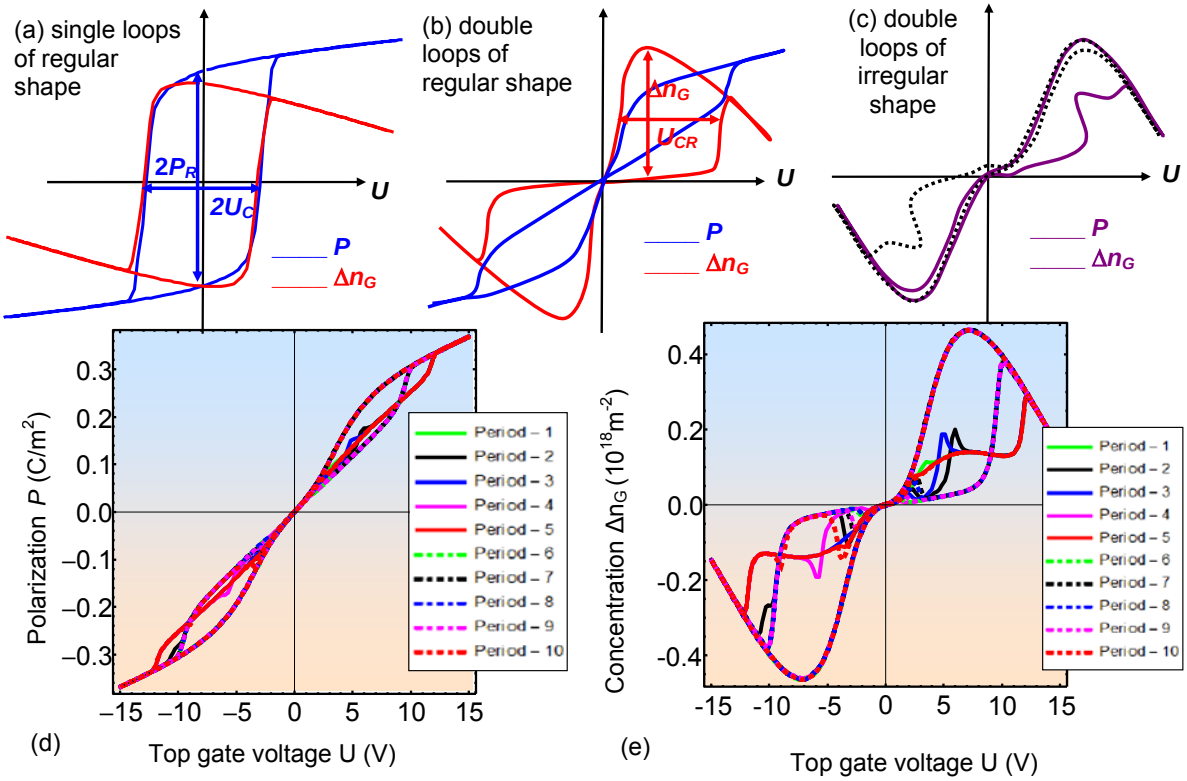

Figure 7. Schematics showing the parameters of polarization $P(U)$ **(a)** and concentration $\Delta n(U)$ **(b)** hysteresis loops. Graph **(c)** schematically shows double loops of irregular shape. Multistable quasi-

chaotic double loops of polarization **(d)** and concentration **(e)** calculated at T=420K and U_{max} = 15 V. The loops "super-period" consisting of 10 period of the gate voltage.

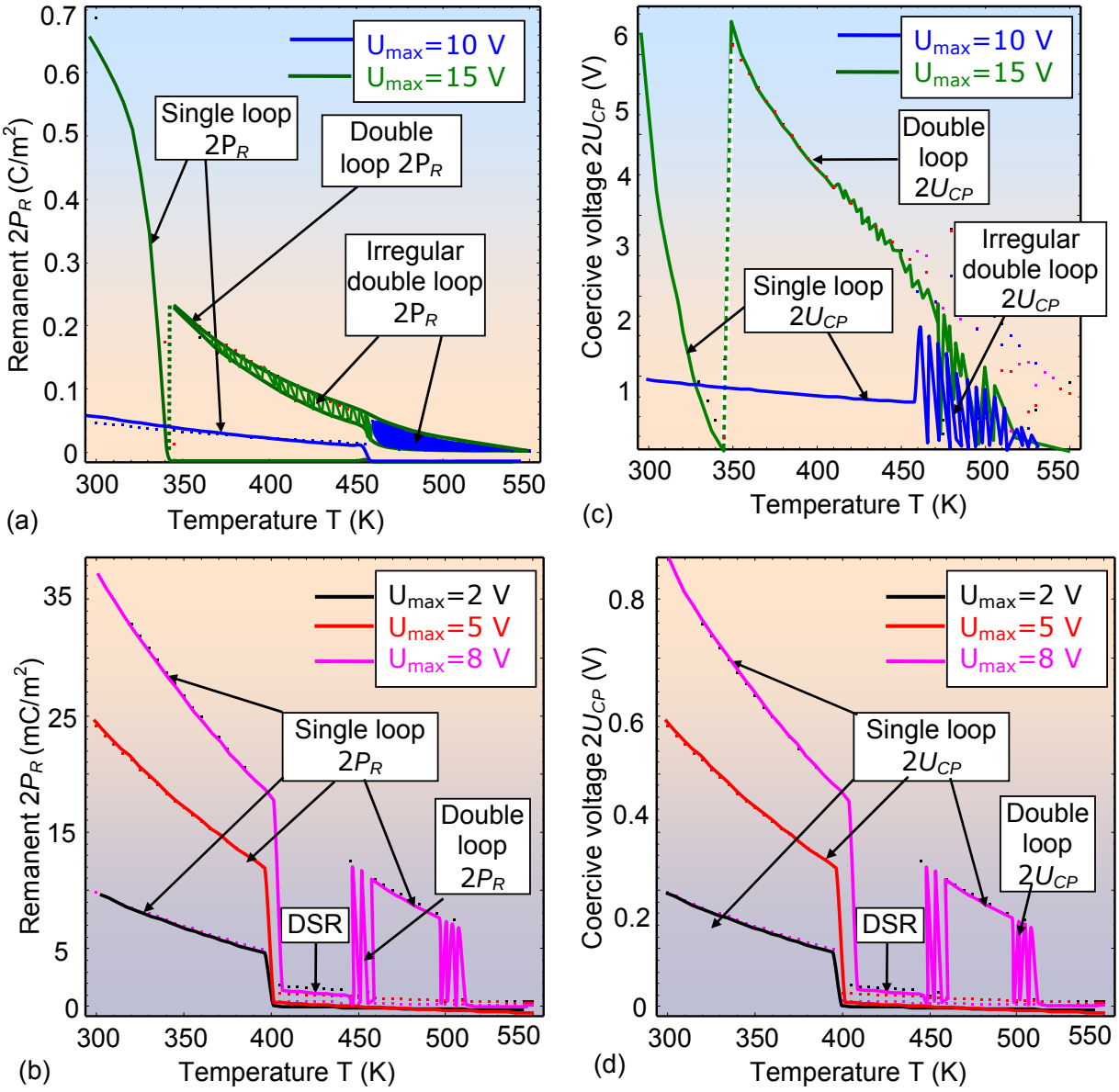

Figure 8. Temperature dependences of the remanent average polarization $P_R(U)$ **(a, b),** and coercive voltage of polarization reversal **(c, d)** calculated for the different amplitudes of the gate voltage U_{max} = (2, 5, 8, 10, 15) V and T_g=1000 s. Other parameters are listed in **Table SI.** Abbreviation "DSR" indicates the region of domain structure rebuilding. Regularly changing parameters (regular curves) of the single loops and oscillating parameters (randomly oscillating curves) of the double loops with regular or irregular shape are shown.

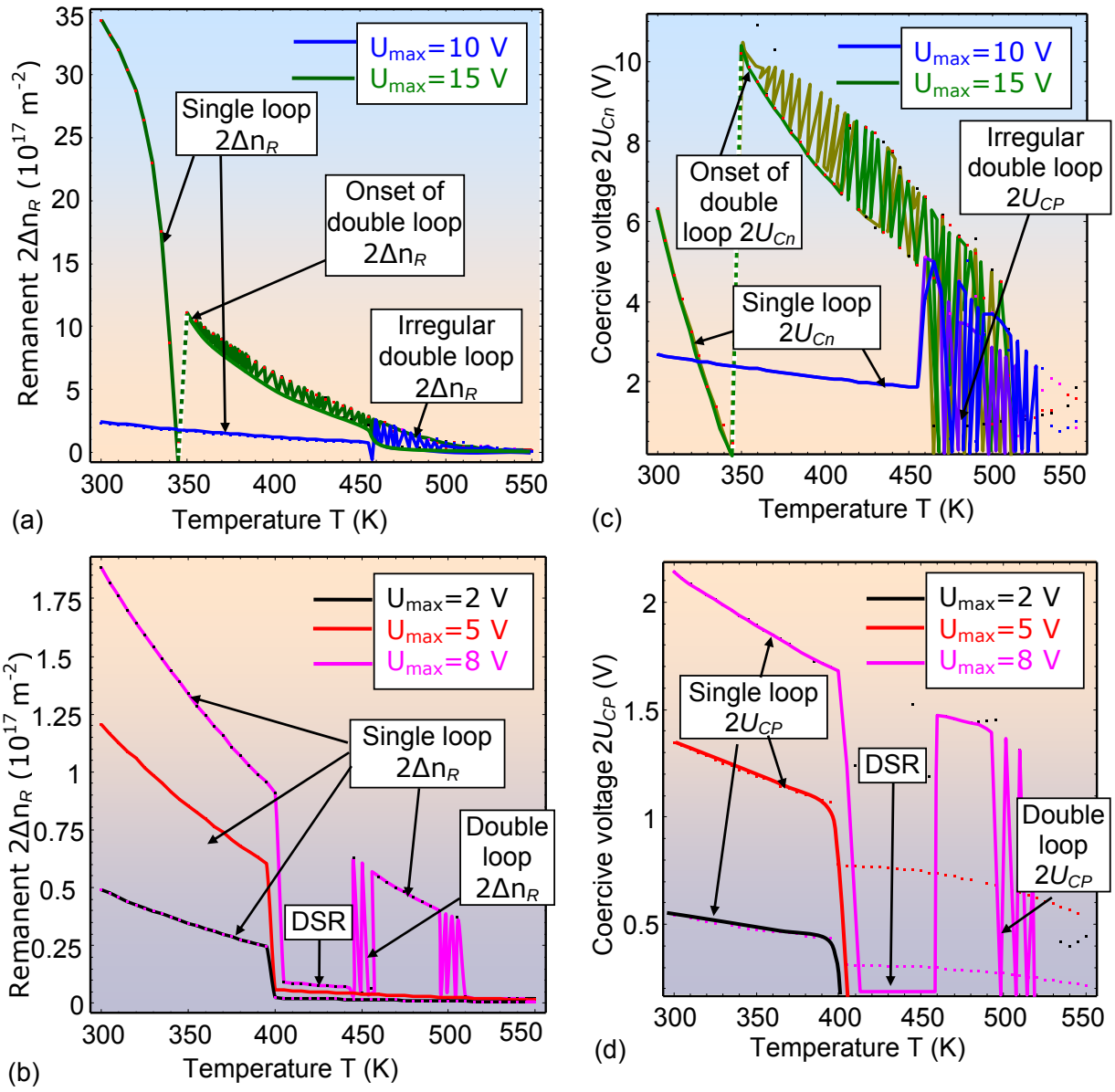

Figure 9. Temperature dependences of the remanent concentration of the carriers in graphene channel $\Delta n_R(U)$ **(a, b)** and coercive voltage of concentration reversal **(c,d)** calculated for the different amplitudes of the gate voltage U_{max} = (2, 5, 8, 10, 15) V and T_g=1000 s. Other parameters are listed in **Table SI.** Abbreviation "DSR" indicates the region of domain structure rebuilding. Regularly changing parameters (regular curves) of the single loops and oscillating parameters (randomly oscillating curves) of the double loops are shown.

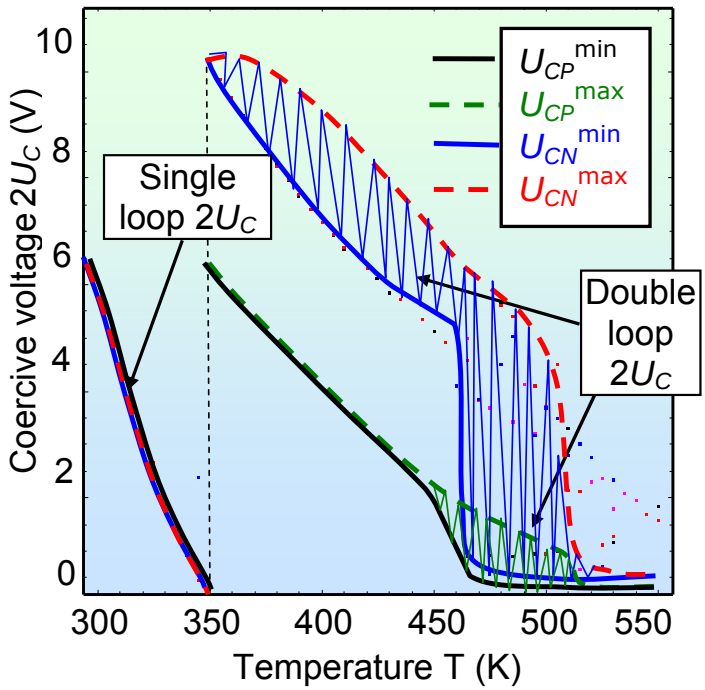

Figure 10. Temperature dependences of the coercive voltage of polarization (curves with labels U_{CP}^{min} and U_{CP}^{max}) and concentration (curves with labels U_{CN}^{min} and U_{CN}^{max}) reversal calculated for the maximal amplitudes of the gate voltage U_{max} = 15 V and T_g=1000 s. Other parameters are listed in **Table SI.** The zigzag-like oscillations of on the coercive fields temperature dependences originated from the quasi-chaotic behavior of the double loops with irregular shape

Note, that the study of the temperature dependence of graphene channel conductance involves the problem how the carriers mean free path depends on temperature [3]. However, for the most common case of dominant carriers scattering mechanism in the channel at the ionized impurities in the substrate it can be demonstrated (see e.g. [3, 28]) that the channel conductance follows the general features of temperature dependence, presented by hysteresis loops in **Figs. 6-7**, and their parameters, analyzed in **Figs. 8-10**. This temperature behavior of the graphene channel conductivity should be taken into account in GFETs operation.

Conclusions

We studied how the temperature evolution of the domain structure in a ferroelectric substrate influences on the distribution of the concentration and type of carrier's in a graphene channel. It was found that the average concentration of carriers in graphene channel reveals the behavior similar to ferroelectric (single hysteresis loops) or antiferroelectric-like (double hysteresis loops) depending on the gate voltage amplitude and temperature. At that the wide temperature range of the double loop existence (about 180 K) is at least 10 times more that the range of double

hysteresis loops existence in the ferroelectric with the first order phase transition to a paraelectric phase.

The physical origin of the single to double antiferroelectric-like loop transition can be explained the voltage behavior of the graphene charge density shown for different temperatures, at that density becomes significantly steeper with the temperature decrease [**Fig.1(b)]**. The graphene charge is responsible for the polarization screening in a ferroelectric substrate. High charge densities (corresponding to high acting electric potential and lower temperatures) can provide an effective screening, and the low ones (corresponding to small potentials and higher temperatures) can provide a weak incomplete screening only. At room and lower temperatures the substrate (PZT film of thickness 75 nm) is in a deep ferroelectric phase, and relatively weak screening of its depolarization field by graphene sheet is enough to support the ferroelectricity in it. Corresponding hysteresis loop is a single one, has a square-like shape with relatively high remnant polarization and coercive voltage. The situation principally changes with the temperature increase, since the film approaches the paraelectric transition. At that the better the screening the higher is the critical thickness of the transition [64-66]. Thus additional screening by graphene carriers is urgently required to maintain the thin film in a ferroelectric state. As one can see from **Fig.1(b)** the screening increase emerges at nonzero potential φ that is in turn proportional to the gate voltage *U*. When the critical voltage corresponds to the screening degree enough to suppress the thickness-induced paraelectric transition, it opens minor loops of polarization, which in turn induce the concentration loops of anti-hysteretic type.

Single and double loops, which have a regular shape, are reproducible at every period of applied voltage, as anticipated. Unexpectedly we revealed the double loops of polarization and concentration, which have irregular shape. They remains irregular as long as the computation takes place, and the voltage position of the different features (jumps, secondary maxima, etc.) changes from one period to another, leading to the impression of quasi-chaotic behavior [**Figs.7(d,e)**]. We established that the physical origin of the "quasi-chaotic" behavior of the polarization and concentration double loops is the strongly nonlinear voltage behavior of the graphene screening charge. The nonlinearity rules the voltage behavior of polarization screening by graphene 2D-layer and at the same time induces the motion of separated domain walls accompanied by the motion of p-n junction along the graphene channel. More detailed analysis of the nonlinear system behavior should be performed within the framework of bifurcation theory [71] that will be the subject of our further studies.

Existence of multi-domain states in a ferroelectric substrate causes inhomogeneous carrier's distribution in graphene channel and lead to formation a set of p-n junctions along

channel. Revealed p-n junctions exist in a wide temperature range below the ferroelectric transition temperature; they vanish in the immediate vicinity of the temperature.

Since the domain walls structure, period and kinetics can be controlled by varying the temperature, we concluded that the considered nano-structures based on graphene-on-ferroelectric elements are promising for the fabrication of new generation of modulators and non-volatile memory units based on the graphene p-n junctions.

Acknowledgements. The publication contains the results of studies conducted by President's of Ukraine grant for competitive projects (grant number F74/25879) of the State Fund for Fundamental Research (A.I.K., A.N.M.). A.N.M. acknowledges the European Union's Horizon 2020 research and innovation programme under the Marie Skłodowska-Curie grant agreement No 778070 and the National Academy of Sciences of Ukraine (projects No. 0118U003535 and 0117U000240). S.V.K. acknowledges the Office of Basic Energy Sciences, U.S. Department of Energy. Part of work was performed at the Center for Nanophase Materials Sciences, which is a DOE Office of Science User Facility.

Authors' contribution. A.I.K. and E.A.E. wrote the codes, performed numerical calculations and presented their results in graphical form, as well as assisted A.N.M. with the interpretation of numerical results. A.N.M. generated the research idea, stated the problem and wrote the manuscript. S.V.K. and M.V.S. working on the manuscript improvement and discussion.

Appendix A. Parametric study of the electric fields

The problem geometry shown in the **Fig. 1(a)** the system of electrostatic equations acquires the form:

$$\Delta\varphi_O = 0, \quad \text{for} \quad -h_O < z < 0, \quad \text{(oxide dielectric layer "}O\text{")} \tag{S.1a}$$

$$\Delta\varphi_{DL} = 0, \quad \text{for} \quad 0 < z < h_{DL}, \quad \text{(dead layer "}d\text{")} \tag{S.1b}$$

$$\left(\varepsilon_{33}^{b}\frac{\partial^2}{\partial z^2}+\varepsilon_{11}^{f}\Delta_{\perp}\right)\varphi_f = \frac{1}{\varepsilon_0}\frac{\partial P_3^f}{\partial z}, \quad \text{for} \quad h_{DL} < z < h_{DL}+h_F. \quad \text{(ferroelectric "}f\text{")} \tag{S.1c}$$

3D-Laplace operator is Δ, 2D-Laplace operator is $\Delta_{\perp}$. Explicit form of the boundary conditions (**BCs**) in z–direction is:

$$\varphi_O(x,y,-h_O) = U(t), \tag{S.2a}$$

$$\varphi_O(x,y,0) = \varphi_{DL}(x,y,0), \qquad D_3^o(x,y,0) - D_3^d(x,y,0) = \sigma_G(x,y,\varphi), \tag{S.2b}$$

$$\varphi_{DL}(x,y,h_{DL}) = \varphi_f(x,y,h_{DL}), \qquad D_3^d(x,y,h_{DL}) - D_3^f(x,y,h_{DL}) = 0, \tag{S.2c}$$

$$\varphi_f(x,y,h_{DL}+h_F) = 0. \tag{S.2d}$$

Let us consider 1D case and suppose that distribution is almost homogeneous inside a wide domain, $P_3 \approx \langle P_3 \rangle$, where the averaging here means the averaging over the domain volume. The assumption is also valid for e.g. **single-domain ferroelectric state**, or in the **central region of a wide domain** the high extrapolation length $\Lambda_{\pm} >> \sqrt{\varepsilon_0 \varepsilon_{33}^b g}$. For the case the solution for potential distribution is:

$$\varphi_O = U - E_O(z - h_{DL} - h_O), \qquad \varphi_{DL} = \Psi - z\,E_{DL}, \qquad \varphi_f = -(h_f + z)E_f. \tag{S.3}$$

Here we introduced designations E_O, E_{DL} and E_f for an electric fields in the top oxide layer, lower dead layer and ferroelectric film. Using the conditions of potentials continuity at the interfaces, one could express the electric field via interface potentials Φ and Ψ as follows:

$$E_O = \frac{\Phi - U}{h_O}, \quad E_{DL} = \frac{\Psi - \Phi}{h_{DL}}, \quad E_f = \frac{-\Psi}{h_f}. \tag{S.4}$$

The interface potentials Φ and Ψ should be determined from the conditions of displacement continuity:

$$\varepsilon_0\varepsilon_{DL}\frac{\Psi - \Phi}{h_{DL}} = \langle P_3 \rangle - \varepsilon_0\varepsilon_b\frac{\Psi}{h_f}, \qquad \varepsilon_0\varepsilon_O\frac{\Phi - U}{h_O} - \varepsilon_0\varepsilon_{DL}\frac{\Psi - \Phi}{h_{DL}} = \sigma(\Phi). \tag{S.5}$$

Averaging of the LGD equation (2) and application of the boundary conditions (3) gives $h_f\left\langle a_3 P_3 + a_{33}P_3^{\,3} + a_{333}P_3^{\,5}\right\rangle + g\left(\left.\frac{P_3}{\Lambda_+}\right|_{z=0} + \left.\frac{P_3}{\Lambda_-}\right|_{z=h_f}\right) = h_f E_f$ and at $\Lambda_\pm >> \sqrt{\varepsilon_0 \varepsilon_{33}^b g}$ it yields to

$$a_3\left\langle P_3\right\rangle + a_{33}\left\langle P_3\right\rangle^3 + a_{333}\left\langle P_3\right\rangle^5 \approx -\frac{\Psi}{h_f}. \tag{S.6}$$

Then the system of nonlinear Eqs.(S.4)-(S.6) and Eq.(1) for $\sigma_G(\Phi)$ in the main text could be reduced to the system of coupled equations for $\left\langle P_3\right\rangle$, Φ and Ψ:

$$\Phi = \frac{h_{DL}}{\varepsilon_{DL}}\left(-\frac{\left\langle P_3\right\rangle}{\varepsilon_0} + \left(\frac{\varepsilon_b}{h_f} + \frac{\varepsilon_{DL}}{h_{DL}}\right)\Psi\right), \tag{S.7a}$$

$$\left(\frac{\varepsilon_b}{h_f} + \frac{\varepsilon_O}{h_O} + \frac{\varepsilon_O}{h_O}\frac{\varepsilon_b}{h_f}\frac{h_{DL}}{\varepsilon_{DL}}\right)\Psi = \frac{\varepsilon_O}{h_O}U + \left(\frac{\varepsilon_O}{h_O}\frac{h_{DL}}{\varepsilon_{DL}} + 1\right)\frac{\left\langle P_3\right\rangle}{\varepsilon_0} + \frac{\sigma_G(\Phi)}{\varepsilon_0}, \tag{S.7b}$$

$$U = \left(1 + \frac{\varepsilon_b}{h_f}\left(\frac{h_{DL}}{\varepsilon_{DL}} + \frac{h_O}{\varepsilon_O}\right)\right)\Psi - \left(\frac{h_{DL}}{\varepsilon_{DL}} + \frac{h_O}{\varepsilon_O}\right)\frac{\left\langle P_3\right\rangle}{\varepsilon_0} - \frac{h_O}{\varepsilon_O}\frac{\sigma_G(\Phi)}{\varepsilon_0}, \tag{S.7c}$$

$$\sigma_G(\Phi) = \frac{4(k_B T)^2 e}{\pi\hbar^2 v_F^2}\sum_{m=1}^{\infty}\frac{(-1)^m}{m^2}\sinh\left[m\left(\frac{e\Phi}{k_B T}\right)\right] \approx \frac{2(k_B T)^2 e}{\pi\hbar^2 v_F^2}\left(\frac{1}{\eta(\Phi)} - \frac{1}{\eta(-\Phi)}\right), \tag{S.7d}$$

$$a_3\left\langle P_3\right\rangle + a_{33}\left\langle P_3\right\rangle^3 + a_{333}\left\langle P_3\right\rangle^5 \approx -\frac{\Psi}{h_f}. \tag{S.7e}$$

The asymptotic series for $\sigma_G(\Phi)$ is converging until $\left|\frac{e\Phi}{k_B T}\right| < 1$, while its approximation with $\eta(\psi) = \exp(\psi) + 2\left(\psi^2 + \frac{\psi}{2} + \frac{2\pi^2}{12-\pi^2}\right)^{-1}$ is valid for all Φ.

From Eqs.(S.7) spontaneous polarization $P_3(U=0)$ induces the charge density $\sigma_G(\Phi)$ in graphene. Equations (S.7) allow us to control the value of electric fields in the oxide and dead layers, since they should be much smaller than the threshold breakdown fields, which are less than 1 V/nm for oxide dielectric (e.g. SiO_2) and less than 0.1 V/nm for a paraelectric dead layer. Below we performed numerical calculations for the parameters listed in **Table S1.**

Table SI. Material parameters used in numerical calculations

Parameter, constant or value	**Numerical value and dimensionality**
oxide dielectric thickness	h_O = 8 nm (typical range 5 – 50 nm)
natural dead layer thickness	h_{DL} = 0.4 nm (typical range 0.2 – 2 nm)
ferroelectric film thickness	h_F = 75 nm (typical range 10 nm – 10 μm)
graphene channel length	*L*=200 nm (32 nm region is shown in figures)

universal dielectric constant	$\varepsilon_0 = 8.85\times10^{-12}$ F/m (e/Vm)
permittivity of the oxide dielectric layer	$\varepsilon_O = 20$ (typical range 10 – 300)
permittivity of the dielectric dead layer	$\varepsilon_{DL} = 100$ (typical range 50 – 500)
Ferroelectric permittivity of the ferroelectric film	$\varepsilon_{33}^f = 500$, $\varepsilon_{11}^f = \varepsilon_{22}^f$=780 (Pb(ZrTi)$O_3$-like)
Background permittivity of the ferroelectric film	$\varepsilon_{11}^b = \varepsilon_{22}^b = \varepsilon_{33}^b = 4$ (Pb(ZrTi)O_3, $BaTiO_3$, or other ferroelectric perovskites)
Landau-Ginzburg-Devonshire potential coefficients	α_T=2.66×10^5 C^{-2}·mJ/K, T_C =666 K (PbZr$_x$Ti$_{1-x}$O$_3$, x ≈ 0.5), P_S^{bulk}=(0.5 – 0.7) C/m^2 b = 1.91×10^8 J C^{-4}·m^5, c = 8.02×10^8 J C^{-6}·m^9
Temperature	T= 300 K; 350 K; 400 K; 450 K; 500 K
dielectric anisotropy of ferroelectric film	$\gamma = \sqrt{\varepsilon_{33}^f / \varepsilon_{11}^f}$ =0.8
extrapolation length	$\Lambda_+ = \Lambda_- = \infty$
Plank constant	$\hbar = 1.056\times10^{-34}$ J·s = 6.583×10^{-16} eV·s
Fermi velocity of electrons in graphene	$v_F \approx 10^6$ m/s

The "reduced" thickness of oxide layer h_O/ε_O is small and the "reduced" thickness of dead layer h_{DL}/ε_{DL} is very small for physically reasonable thicknesses $h_{O,DL}$ and relative permittivities $\varepsilon_{O,DL}$ ranges listed in **Table S1. Figures S1-S3** illustrate the dependences of the positive solution for spontaneous polarization $\langle P_3 \rangle$ and induced negative charge σ_G on the parameter h_O/ε_O, calculated for several values of the ratio h_{DL}/ε_{DL} varying in the range (0.002 – 0.03), temperatures T=300, 350, 400 and 450 K. Negative solutions for spontaneous polarization $-\langle P_3 \rangle$ and positive graphene charge $-\sigma_G$ are not shown, since the curves are symmetric to the curves $+\langle P_3 \rangle$ and $+\sigma_G$ with respect to x-axes.

One can see from the **Figs.S1** and **S3(a)** that $\langle P_3 \rangle$ decreases with h_O/ε_O increasing. However the dependence of $\langle P_3 \rangle$ on h_O/ε_O becomes non-monotonic and then pronouncedly bistable (two positive values of $\langle P_3 \rangle$ corresponds to one value of h_O/ε_O) with h_{DL}/ε_{DL} decrease and temperature decrease [compare **Figs.S1(a)-(d)**]. The polarization disappears when the ratio h_O/ε_O becomes higher that some critical value, which in turn increases with the ratio h_{DL}/ε_{DL} decrease.

One can see from the **Figs.S2** and **S3(b)** that σ_G firstly increases and then decreases with h_O/ε_O increasing. Hence the dependence of σ_G on h_O/ε_O is always non-monotonic and becomes pronouncedly bistable with temperature decrease (two negative values of σ_G corresponds to one value of h_O/ε_O) with h_{DL}/ε_{DL} decrease [compare **Figs.S2(a)-(d)**]. The

graphene charge disappears when the ratio h_O/ε_O becomes higher that some critical value, which in turn increases with the ratio h_{DL}/ε_{DL} decrease.

Let us underline that the carrier density in graphene induced by ferroelectric substrate can be substantially lower than the polarization of the ferroelectric layer (compare $\langle P_3 \rangle$=0.5 C/m^2 and σ_G = –0.3 C/m^2 at 300 K; $\langle P_3 \rangle$=0.4 C/m^2 and σ_G = –0.03 C/m^2 at 500 K).

Notably the bistability regions of $\langle P_3 \rangle$ and σ_G corresponds to the appearance of contraction and other complex features at the polarization and charge hysteresis loops, at that the charge bistability regions are much wider and pronounced. The bistability regions are wider and more pronounced at room and lower temperatures; they becomes narrow and vanishes with the temperature increase (compare plots (a) for 300 K with plots (b)-(d) for higher temperatures).

From **Figs. S1(a)** and **S2(a)** the bistability region of spontaneous polarization and graphene charge appears for the ratio h_O/ε_O within the range $0.03\text{nm} < h_O/\varepsilon_O < 1\,\text{nm}$ at 300 K. The bistability region exists at h_{DL}/ε_{DL} <0.03 nm.

Hence we select the values $h_{DL} = 0.4\text{nm}$ and $\varepsilon_{DL} = 100$ (corresponding to $h_{DL}/\varepsilon_{DL} = 0.004\,\text{nm}$), $h_O = 0.8$ nm and $\varepsilon_O = 20$ (corresponding to the ratio $h_O/\varepsilon_O = 0.04\,\text{nm}$) for numerical modeling in the main text (see **Figs.2-10** and **Table S1)** not only because they correspond to realistic experimental situation, but primary because our parametric study presented in this **Appendix** predicts unusual hysteresis properties of $\langle P_3 \rangle$ and σ_G for these values**.**

The top oxide thickness h_O can vary in the experimental range (5 – 50) nm and h_{DL} usually does not exceed several nm. To study the parameters h_O and h_{DL} effect on the hysteresis loops we performed numerical calculations, which results are shown in **Figs.S4. Figure S4(a)** shows how the charge concentration in graphene changes with h_O increase at fixed other parameters. One can see from the figure the expected and trivial result – the loops become much slimmer with h_O increase from 8 nm to 25 nm at fixed ε_O=80. **Figure S4(b)** shows how the charge concentration in graphene changes with the increase of h_{DL} from 0.5 nm to 2.5 nm at fixed other parameters. From the figure the expected result is that the loops looses their ferroelectric-like shape, becomes horizontally tilted and elliptic-like with h_{DL} increase from 0.5 nm to 2.5 nm at fixed ε_{DL}=80.

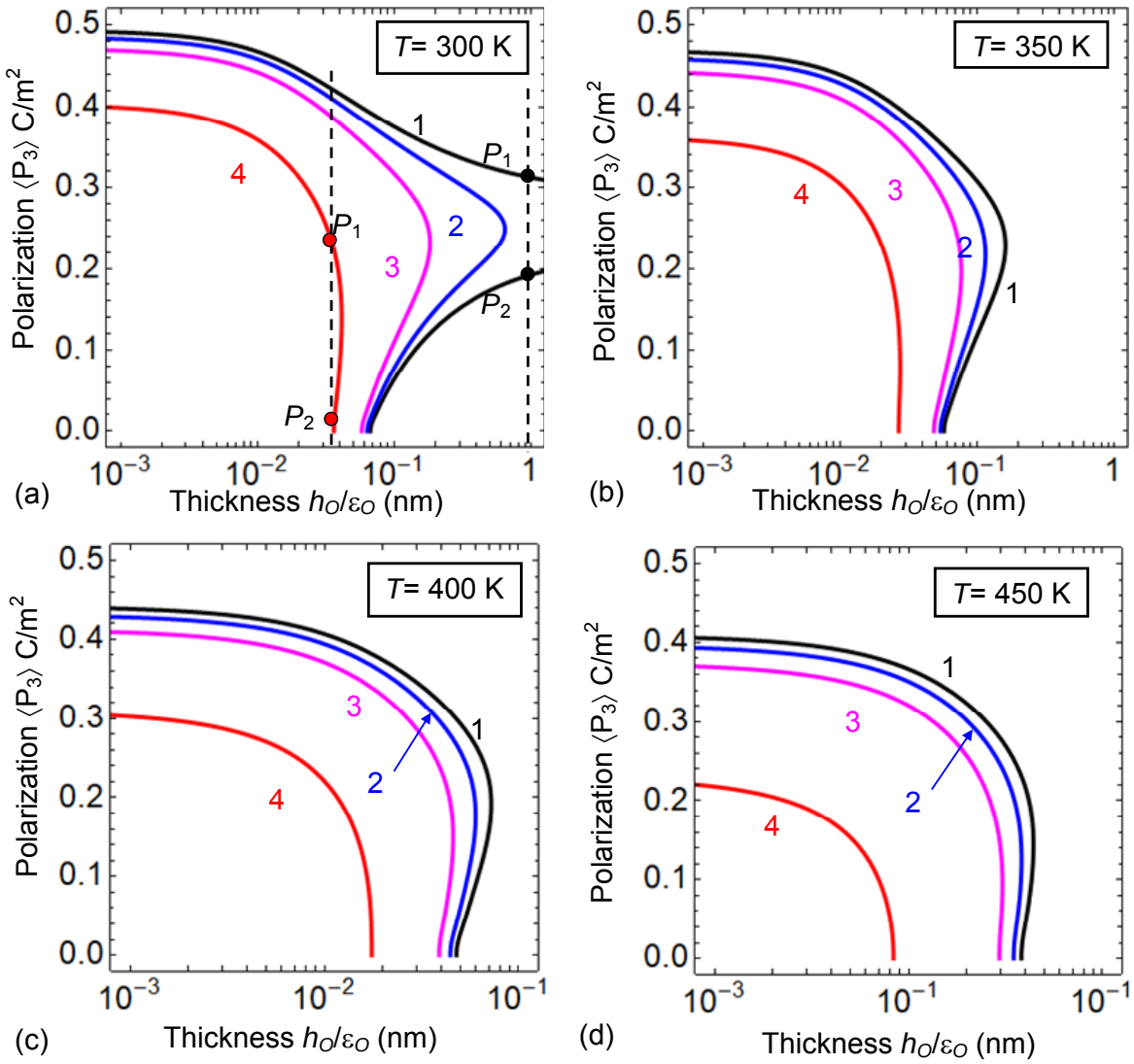

Figure S1. Dependences of polarization $\langle P_3 \rangle$ on the reduced thickness h_O/ε_O, calculated for fixed values of h_{DL}/ε_{DL} = 0.002, 0.005, 0.01 nm and 0.03 nm (see curves 1, 2, 3 and 4) under zero gate voltage $U = 0$ at *T*=300, 350, 400 and 450 K **(a, b, c** and **d)**. Other parameters are listed in **Table S1**.

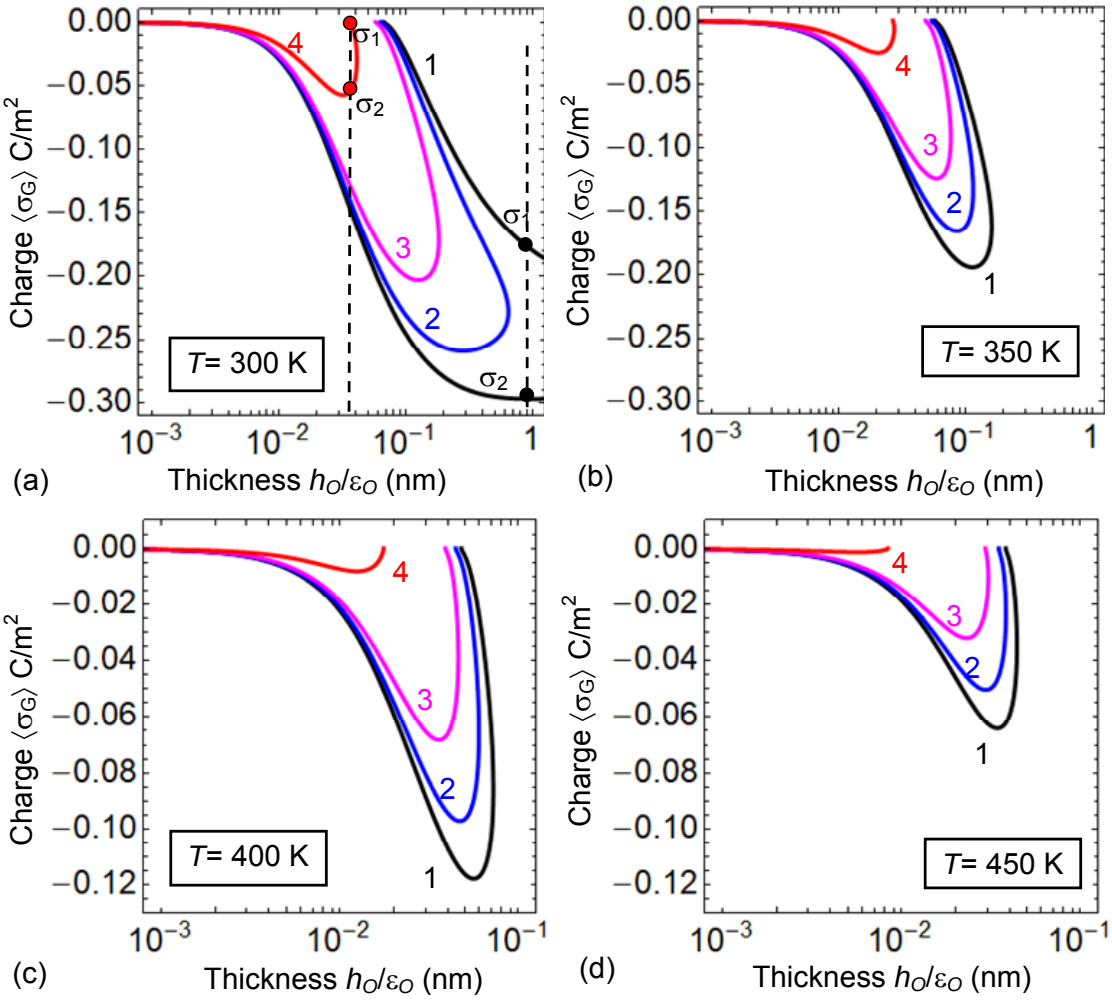

Figure S2. Dependences of graphene charge $\sigma_G(\Phi)$ on the reduced thickness h_O/ε_O, calculated for fixed values of h_{DL}/ε_{DL} =0.002, 0.005, 0.01 nm and 0.03 nm (see curves 1, 2, 3 and 4) under zero gate voltage $U = 0$ at T=300, 350, 400 and 450 K **(a, b, c** and **d)**. Other parameters are listed in **Table S1**.

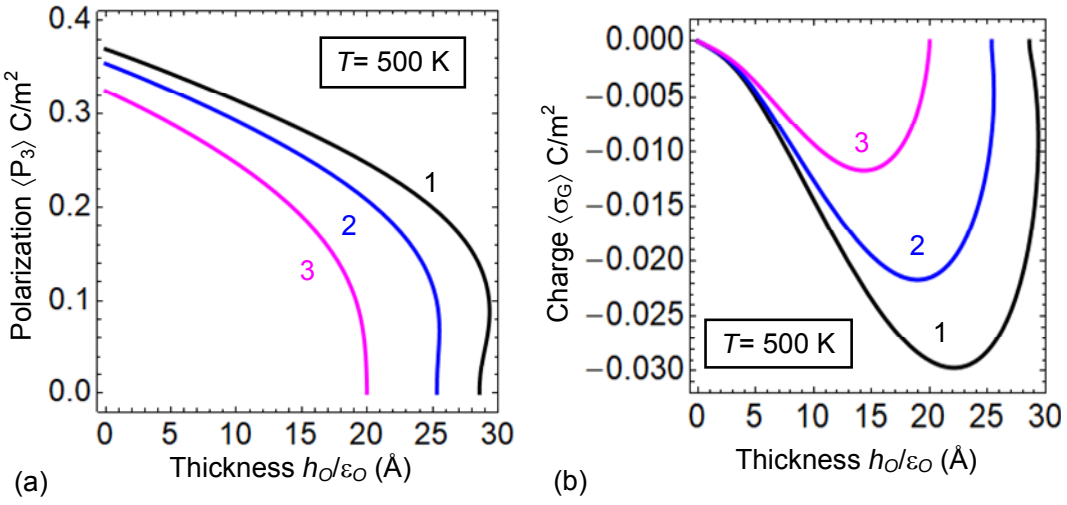

Figure S3. Dependences of polarization $\langle P_3 \rangle$ **(a)** and graphene charge $\sigma_G(\Phi)$ **(b)** on the reduced thickness h_O/ε_O, calculated for fixed values of h_{DL}/ε_{DL} =0.002, 0.005, 0.01 nm (see curves 1, 2, 3)

under zero gate voltage $U = 0$ at T=500 K **(a, b, c** and **d)**. The spontaneous polarization $\langle P_3 \rangle$ and corresponding charge $\sigma_G(\Phi)$ are absent for h_{DL}/ε_{DL} =0.03 nm. Other parameters are listed in **Table S1**.

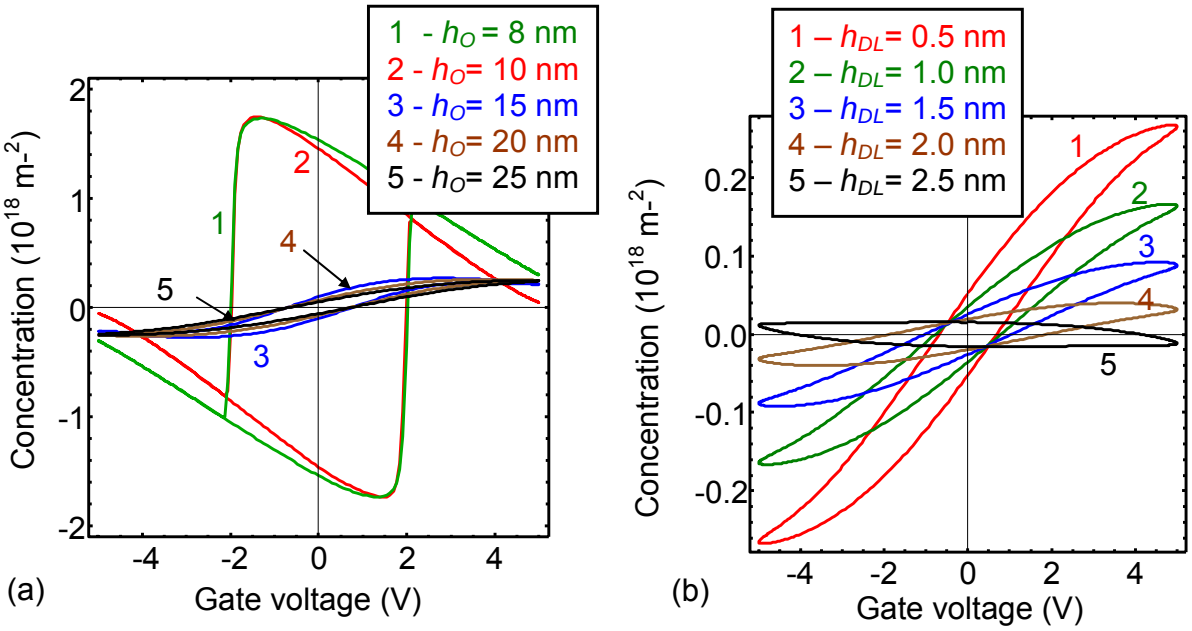

Figure S4. (a) The charge concentration in graphene changes with h_O increase from 8 nm to 25 nm at fixed ε_O =20, temperature 300 K, gate voltage 5V, period = 1000s, ε_{DL}=80 and h_{DL}=0.4 nm. **(b)** The charge concentration in graphene changes with h_{DL} increase from 0.5 nm to 2.5 nm at fixed ε_{DL}=80, temperature 300 K, gate voltage 5V, period = 1000s, ε_O =20 and h_O =8 nm.

References

[1] K. Novoselov, *A.* Geim, S. Morozov, *D.* Jiang, Y. Zhang, S. Dubonos, *I.* Grigorieva, *A.* Firsov, "Electric Field Effect in Atomically Thin Carbon Films", Science, **306**, 666 (2004)

[2] A.Geim. "Graphene: status and prospects." Science, **324**, 1530 (2009)

[3] S. Das Sarma, Shaffique Adam, E.H. Hwang, E.Rossi, "Electronic transport in two-dimensional graphene." Rev. Mod. Phys. **83**, 407 (2011)

[4] Gerardo G. Naumis, Salvador Barraza-Lopez, Maurice Oliva-Leyva, and Humberto Terrones. "Electronic and optical properties of strained graphene and other strained 2D materials: a review." *Reports on Progress in Physics* (2017). *arXiv preprint arXiv:1611.08627* (2016).

[5] Schedin, F.; Geim, A. K.; Morozov, S. V.; Hill, E. W.; Blake, P.; Katsnelson, M. I.; Novoselov, K. S. Detection of individual gas molecules adsorbed on graphene. *Nature Materials* **2007**, 6, 652-655.

[6] Guang-Xin, Yi Zheng, Sukang Bae, Chin Yaw Tan, Orhan Kahya, Jing Wu, Byung Hee Hong,Kui Yao and Barbaros Özyilmaz. Graphene – Ferroelectric Hybrid Structure for Flexible Transparent Electrodes. *ACS Nano*, **2012**, *6* (5), 3935–3942

[7] Zhang, X.-W.; Xie, D.; Xu, J.-L.; Zhang, C.; Sun, Y.-L.; Zhao, Y.-F.; Li, X.; Li, X.-M.; Zhu, H.-W.; Chen, H.-M.; Chang, T.-C. Temperature-dependent electrical transport properties in graphene/Pb($Zr_{0.4}Ti_{0.6}$)O_3 field effect transistors. *Carbon* **2015**, 93, 384 –392.

[8] Rajapitamahuni, A.; Hoffman, J.; Ahn, C. H.; Hong, X. Examining Graphene Field Effect Sensors for Ferroelectric Thin Film Studies. *Nano Letters* **2013**, 13, 4374-4379.

[9] Yusuf, M.H.; Nielsen, B.; Dawber, M.; Du, X. Extrinsic and Intrinsic Charge Trapping at the Graphene/Ferroelectric Interface. *Nano Letters* **2014**, 14, 5437-5444.

[10] J. Scott Bunch, Arend M. van der Zande, Scott S. Verbridge, Ian W. Frank, David M. Tanenbaum, Jeevak M. Parpia, Harold G. Craighead, Paul L. McEuen. Electromechanical Resonators from Graphene Sheets. Science. 2007 Jan 26;315(5811):490-3.

[11] K. I. Bolotin, K. J. Sikes, J. Hone, H. L. Stormer, and P. Kim. Temperature-Dependent Transport in Suspended Graphene. PRL 101, 096802 (2008)

[12] Bolotin KI, Ghahari F, Shulman MD, Stormer HL, Kim P. Observation of the fractional quantum Hall effect in graphene. Nature. 2009 Nov 12;462(7270) .

[13] Xu Du, Ivan Skachko, Fabian Duerr, Adina Luican and Eva Y. Andrei. Fractional quantum Hall effect and insulating phase of Dirac electrons in graphene. Nature 462, 192 – 195 (12 november 2009).

[14] Bao W, Miao F, Chen Z, Zhang H, Jang W, Dames C, Lau CN. Controller ripple texturing of suspended grapheme and ultratin graphite membranes. Nat Nanotechnol. 2009 Sep;4(9):562-6.

[15] Eduardo V. Castro, H. Ochoa, M. I. Katsnelson, R. V. Gorbachev, D. C. Elias, K. S. Novoselov, A. K. Geim, and F. Guinea. Limits on Charge Carrier Mobility in Suspended Graphene due to Flexural Phonons. PRL 105, 266601 (2010)

[16] Yi Zheng, Guang-Xin Ni, Chee-Tat Toh, Chin-Yaw Tan, Kui Yao, Barbaros Özyilmaz. "Graphene field-effect transistors with ferroelectric gating." Phys. Rev. Lett. **105**, 166602 (2010).

[17] M. Humed Yusuf, B. Nielsen, M. Dawber, X. Du., "Extrinsic and intrinsic charge trapping at the graphene/ferroelectric interface." Nano Lett, **14** (9), 5437 (2014).

[18] Xia Hong, Emerging ferroelectric transistors with nanoscale channel materials: the possibilities, the limitations, Journal of Physics: Condensed Matter **28** (10), 103003 (2016)

[19] V. Cheianov, V. Falko, "Selective transmission of Dirac electrons and ballistic magnetoresistance of n−p junctions in graphene." Phys.Rev.B, **74**, 041403 (2006)

[20] J.R.Williams, L.DiCarlo, C.M.Marcus, "Quantum Hall effect in a gate-controlled pn junction of graphene." Science, **317**, 638 (2007)

[21] Barbaros Ozyilmaz, Pablo Jarillo-Herrero, Dmitri Efetov, Dmitry A. Abanin, Leonid S. Levitov, and Philip Kim. Electronic Transport and Quantum Hall Effect in Bipolar Graphene p−n−p Junctions, Physical Review Letters. 99, 166804(2007).

[22] C.W.Beenakker, “Andreev reflection and Klein tunneling in graphene.” Rev.Mod.Phys. **80**, 1337 (2008).

[23] M. I. Katsnelson, K. S. Novoselov, and A. K. Geim, “Chiral tunnelling and the Klein paradox in graphene”. Nat. Phys. **2**, 620 (2006).

[24] V. V. Cheianov, V. I. Falko, and B. L. Altshuler, The Focusing of Electron Flow and a Veselago Lens in Graphene *p-n* Junctions. Science **315**, 1252 (2007).

[25] J. H. Hinnefeld, Ruijuan Xu, S. Rogers, Shishir Pandya, Moonsub Shim, L. W. Martin, N. Mason. "Single Gate PN Junctions in Graphene-Ferroelectric Devices." *arXiv preprint arXiv:1506.07138* (2015).

[26] C. Baeumer, D. Saldana-Greco, J. M. P. Martirez, A. M. Rappe, M. Shim, L. W. Martin. "Ferroelectrically driven spatial carrier density modulation in graphene." *Nature communications* **6**, Article number: 6136; doi:10.1038/ncomms7136 (2015).

[27] N.M.Zhang, M.M.Fogler, "Nonlinear screening and ballistic transport in a graphene p − n junction." Phys. Rev. Lett., **100**, 116804 (2008)

[28] Yu. A. Kruglyak, M. V. Strikha. Generalized Landauer – Datta – Lundstrom Model in Application to Transport Phenomena in Graphene. Ukr. J.Phys. Reviews, **10**, 3 (2015)

[29] A.I. Kurchak, M.V. Strikha, "Conductivity of graphene on ferroelectric PVDF-TrFE". Ukr. J. Phys. **59**, 622 – 627 (2014).

[30] Anatolii I. Kurchak, Anna N. Morozovska, and Maksym V. Strikha. Hysteretic phenomena in GFET: general theory and experiment. Journal of Applied Physics, **122**, 044504 (2017)

[31] Woo Young Kim, Hyeon-Don Kim, Teun-Teun Kim, Hyun-Sung Park, Kanghee Lee, Hyun Joo Choi, Seung Hoon Lee, Jaehyeon Son, Namkyoo Park, and Bumki Min. "Graphene-ferroelectric metadevices for nonvolatile memory and reconfigurable logic-gate operations." *Nature communications* **7**, Article number: 10429; doi:10.1038/ncomms10429 (2016).

[32] A. N. Morozovska, M. V. Strikha. "Pyroelectric origin of the carrier density modulation at graphene-ferroelectric interface." J. Appl. Phys. **114**, 014101 (2013).

[33] A. N. Morozovska, E. A. Eliseev, A. V. Ievlev, O. V. Varenyk, A. S. Pusenkova, Ying-Hao Chu, V. Ya. Shur, M. V. Strikha, S. V. Kalinin, "Ferroelectric domain triggers the charge modulation in semiconductors." Journal of Applied Physics, **116**, 066817 (2014).

[34] A. N. Morozovska, A. S. Pusenkova, O.V. Varenyk, S.V. Kalinin, E.A. Eliseev, and M. V. Strikha, “Finite size effects of hysteretic dynamics in multi-layer graphene on ferroelectric”. Physical Review B **91**, 235312 (2015).

[35] Anna N. Morozovska, Eugene A. Eliseev, and Maksym V. Strikha. Ballistic conductivity of graphene channel with p-n junction on ferroelectric domain wall. Applied Physics Letters 108, 232902 (2016)

[36] Maksym V. Strikha and Anna N. Morozovska. Limits for the graphene on ferroelectric domain wall p-n-junction rectifier for different regimes of current. J. Appl. Phys. **120**, 214101 (2016)

[37] A. I. Kurchak, E. A. Eliseev, S. V. Kalinin, M. V. Strikha, A. N. Morozovska. (http://arxiv.org/abs/1703.06500)

[38] I. Jung, J.Y. Son, “A nonvolatile memory device made of a graphene nanoribbon and a multiferroic BiFeO3 gate dielectric layer”, *Carbon.* V. 50. P. 3854-8 (2012)

[39] J.R. Whyte, J.M. Gregg "A diode for ferroelectric domain-wall motion". Nature Communications, **6**, Article number: 7361 (2015). DOI: 10.1038/ncomms8361

[40] Seyoung Kim, Junghyo Nah, Insun Jo, Davood Shahrjerdi, Luigi Colombo, Zhen Yao, Emanuel Tutuc, and Sanjay K. Banerjee, Realization of a high mobility dual-gated graphene field-effect transistor with Al_2O_3 dielectric, Applied Physics Letters **94**(6), 062107 (2009).

[41] Ke Zou, Xia Hong, Derek Keefer, and Jun Zhu, Deposition of high-quality HfO_2 on graphene and the effect of remote oxide phonon scattering, Physical review letters **105**(12), 126601 (2010).

[42] Xia Hong, Kaiqi Zou, A. M. DaSilva, C. H. Ahn, and J. Zhu, Integrating functional oxides with graphene. Solid State Communications **152**(15), 1365 (2012).

[43] A. K. Tagantsev and G. Gerra. Interface-induced phenomena in polarization response of ferroelectric thin films. J. Appl. Phys. 100, 051607 (2006).

[44] A. K. Tagantsev, M. Landivar, E. Colla, and N. Setter. Identification of passive layer in ferroelectric thin films from their switching parameters. J. Appl. Phys. 78, 2623 (1995).

[45] G. Rupprecht and R.O. Bell, Dielectric constant in paraelectric perovskite. Phys. Rev. 135, A748 (1964).

46 Ivan S. Vorotiahin, Eugene A. Eliseev, Qian Li, Sergei V. Kalinin, Yuri A. Genenko and Anna N. Morozovska. Tuning the Polar States of Ferroelectric Films via Surface Charges and Flexoelectricity. Acta Materialia 137 (15), 85–92 (2017)

47 Eugene A. Eliseev, Ivan. S. Vorotiahin, Yevhen M. Fomichov, Maya D. Glinchuk, Sergei V. Kalinin, Yuri A. Genenko, and Anna N. Morozovska. Defect driven flexo-chemical coupling in thin ferroelectric films. Physical Review B, 97, 024102 (2018)

[48] P. Nemes-Incze, Z. Osváth, K. Kamarás, and L. P. Biró. "Anomalies in thickness measurements of graphene and few layer graphite crystals by tapping mode atomic force microscopy." *Carbon* **46**, no. 11: 1435-1442 (2008).

[49] Elton J.G. Santos, "Electric Field Effects on Graphene Materials." In *Exotic Properties of Carbon Nanomatter*, pp. 383-391. Springer Netherlands, Dordrecht, 2015.

[50] J. Hlinka and P. Márton, Phenomenological model of a 90° domain wall in BaTiO3-type ferroelectrics. Phys. Rev. B 74, 104104 (2006).

[51] L. D. Landau, and I. M. Khalatnikov. "On the anomalous absorption of sound near a second order phase transition point." Dokl. Akad. Nauk SSSR, vol. 96, pp. 469-472 (1954).

[52] R. Kretschmer and K.Binder. "Surface effects on phase transitions in ferroelectrics and dipolar magnets." Phys. Rev. B **20**, 1065 (1979).

[53] Chun-Lin Jia, Valanoor Nagarajan, Jia-Qing He, Lothar Houben, Tong Zhao, Ramamoorthy Ramesh, Knut Urban & Rainer Waser, "Unit-cell scale mapping of ferroelectricity and tetragonality in epitaxial ultrathin ferroelectric films." Nature Materials, **6**. 64 (2007).

[54] E.A. Eliseev, A.N. Morozovska, S.V. Kalinin, Y.L. Li, Jie Shen, M.D. Glinchuk, L.Q. Chen, V. Gopalan. Surface Effect on Domain Wall Width in Ferroelectrics. J. Appl. Phys. 106, 084102 (2009).

[55] S.V. Kalinin, A.N. Morozovska, Long Qing Chen, Brian J. Rodriguez. Local polarization dynamics in ferroelectric materials. Rep. Prog. Phys. 73, 056502-1-67 (2010).

[56] J Wang, S.Q. Shi, L.-Q. Chen, Y. Li, T.Y. Zhang. Phase-field simulations of ferroelectric/ferroelastic polarization switching. Acta Materialia 52 (3), 749-764 (2004)

[57] S Choudhury, Y.L. Li, CE Krill III, L.-Q. Chen. Phase-field simulation of polarization switching and domain evolution in ferroelectric polycrystals. Acta Materialia 53 (20), 5313-5321 (2005)

[58] Z-G. Ban, S. P. Alpay, and J. V. Mantese. "Fundamentals of graded ferroic materials and devices." Phys. Rev. B **67**, no. 18 (2003): 184104.

[59] S. Zhong, Z-G. Ban, S.P. Alpay, and J.V. Mantese. "Large piezoelectric strains from polarization graded ferroelectrics." Appl. Phys. Lett. **89**, no. 14 (2006): 142913.

[60] I.B. Misirlioglu, S.P. Alpay. Compositionally graded ferroelectrics as wide band gap semiconductors: Electrical domain structures and the origin of low dielectric loss. Acta Materialia 122, 266-276 (2017)

[61] James F. Scott, *Ferroelectric Memories,* Springer Series in Advanced Microelectronics. Vol. 3 (2000). ISBN: 978-3-540-66387-4.

[62] P. Zubko, D. J. Jung, and J. F. Scott. Space charge effects in ferroelectric thin films. Journal of Applied Physics 100, 114112 (2006)

[63] Ivan S. Vorotiahin, Eugene A. Eliseev, Qian Li, Sergei V. Kalinin, Yuri A. Genenko and Anna N. Morozovska. Tuning the Polar States of Ferroelectric Films via Surface Charges and Flexoelectricity. Acta Materialia **137** (15), 85–92 (2017)

[64] Tilley D.R. Finite-size effects on phase transitions in ferroelectrics. Ferroelectic Thin Films. ed. C. Paz de Araujo, J.F.Scott and G.W. Teylor.-Amsterdam: Gordon and Breach, 1996.-P.11-4

[65] E.A. Eliseev, A.N. Morozovska. General approach to the description of the size effect in ferroelectric nanosystems. *The Journal of Materials Science*. 44, № 19, 5149-5160 (2009).

[66] Eugene A. Eliseev, Ivan. S. Vorotiahin, Yevhen M. Fomichov, Maya D. Glinchuk, Sergei V. Kalinin, Yuri A. Genenko, and Anna N. Morozovska. Defect driven flexo-chemical coupling in thin ferroelectric films. (http://arxiv.org/abs/1708.00904)

[67] A.K. Tagantsev, L.E. Cross, and J. Fousek. Domains in ferroic crystals and thin films. New York: Springer, 2010.

[68] P. Maksymovych, S. Jesse, M. Huijben, R. Ramesh, A.N. Morozovska, S. Choudhury, L.-Q. Chen, A.P. Baddorf, S.V. Kalinin. Intrinsic nucleation mechanism and disorder effects in polarization switching on ferroelectric surfaces. Phys. Rev. Lett. 102, №1, 017601 (2009).

[69] A.N. Morozovska, E.A. Eliseev, Yulan Li, S.V. Svechnikov, P. Maksymovych, V.Y. Shur, Venkatraman Gopalan, Long-Qing Chen, and S.V. Kalinin. Thermodynamics of nanodomain formation and breakdown in Scanning Probe Microscopy : Landau-Ginzburg-Devonshire approach. Phys. Rev. B. 80, 214110 (2009)

[70] Vasudeva Rao Aravind, A.N. Morozovska, S. Bhattacharyya, D. Lee, S. Jesse, I. Grinberg, Y.L. Li, S. Choudhury, P. Wu, K. Seal, A.M. Rappe, S.V. Svechnikov, E.A. Eliseev, S.R. Phillpot, L.Q. Chen, Venkatraman Gopalan, S.V. Kalinin. Correlated polarization switching in the proximity of a 180° domain wall. Phys. Rev. B 82, 024111-1-11 (2010).

[71] Arnold V.I. Theory of catastrophes, 128 p. Moscow: Nauka (1990) In Russian. ISBN 5-02-014271-9